



This document is a postprint version of an article published in The Journal of Nutritional Biochemistry© Elsevier after peer review. To access the final edited and published work see <https://doi.org/10.1016/j.jnutbio.2020.108393>

Document downloaded from:



1 Molecular phenomics of a high-calorie diet-induced porcine model of

2 prepubertal obesity

3 Mariona Jové^{1*}, Joan Tibau^{2*#}, José CE Serrano¹, Rebeca Berdún¹, María Rodríguez-Palmero³, Maria
4 Font-i-Furnols², Anna Cassanyé¹, Reyna Rodríguez-Mortera¹, Joaquim Sol¹, Helene Rassendren¹, Emma
5 Fàbrega², Anna Crescenti^{4,5}, Anna Castell^{4,5}, Mònica Sabater^{6,7,8}, Francisco J Ortega^{6,7,8}, Meritxell Martin-
6 Gari¹, Raquel Quintanilla⁹, Joaquim Puigjaner³, Jose Antonio Moreno³, Joan Prat¹, Lluís Arola^{4,10}, Josep
7 Manuel Fernández-Real^{6,7,8}, Reinald Pamplona¹ and Manuel Portero-Otin^{1#}

8 ¹NUTREN-Nutrigenomics Fisiopatologia Metabòlica, Universitat de Lleida-IRBLleida, E25196 Lleida, Spain;

9 ²Animal Breeding and Genetics Programme, Institute for Research and Technology in Food and Agriculture
10 (IRTA), Finca Camps i Armet, E17121, Monells, Spain; ³Laboratorios Ordesa S.L., Barcelona Science Park

11 , 08028 Barcelona, Spain; ⁴Nutrition and Health Unit, EURECAT-Technology Centre of Catalonia, Reus,
12 Spain; ⁵Nutrition and Health Research Group, EURECAT-Technology Centre of Catalonia, Reus, Spain;

13 ⁶CIBEROBN and Instituto de Salud Carlos III (ISCIII), Madrid, Spain; ⁷Institut d'Investigació Biomèdica de
14 Girona (IdIBGi), Girona, Spain; ⁸Department of Diabetes, Endocrinology and Nutrition (UDEN), Hospital of

15 Girona "Dr Josep Trueta", Girona, Spain; ⁹Product Quality Program, Institute for Research and Technology
16 in Food and Agriculture (IRTA), Finca Camps i Armet, E17121, Monells, Girona, Spain; ¹⁰Nutrigenomics

17 Research Group, Department of Biochemistry and Biotechnology, Universitat Rovira i Virgili, Tarragona,
18 Spain

19 *Both authors should be considered first authors

20 E-mail:

21 MJ: mariona.jove@mex.udl.cat, JT: joan.tibau@irta.cat, JCES: jeserrano@mex.udl.cat, RB:

22 rebecaberdun@gmail.com, MRP: maria.rodriguez@ordesa.es, MFF: maria.font@irta.cat, AC:

23 annakasa4@gmail.com, RRM: ln.reynarm@gmail.com, JS: jkim173@gmail.com, HR:

24 ln.rassendren@gmail.com, EF: emma.fabrega@irta.cat, AC: anna.crescenti@eurecat.org, ACastell:

25 anna.castell@eurecat.org, MS: msabater@idibgi.org, FJO: fortega@idibgi.org, MMG:

26 meritxell.martin@udl.cat, RQ: Raquel.quintanilla@irta.cat, JP: Joaquim.puigjaner@ordesa.es, JAMM:

27 joseA.moreno@ordesa.es, JPrat: joan.prat@mex.udl.cat, LA: lluis.arola@urv.cat, JMFR:

28 jmfreal@idibgi.org, RP: reinald.pamplona@mex.udl.cat, MPO: manuel.portero@mex.udl.cat

29 **Running title: *Characterization of porcine early obesity***

30 **Address for correspondence:** #To whom correspondence should be addressed at Animal Breeding and
31 Genetics Programme, Institute for Research and Technology in Food and Agriculture (IRTA), Finca Camps
32 i Armet, E17121, Monells, Spain (Joan.Tibau@irta.cat) or Fisiopatologia Metabòlica, Universitat de Lleida-

33 IRBLleida, Edifici Biomedicina I, Avda Rovira Roure, 80 E25196 Lleida, Spain
34 (manuel.portero@mex.udl.cat)

35 **Grants**

36 Supported by CDTI (Centro para el Desarrollo Tecnológico e Industrial, Spain), Project reference: IPT-
37 20111008, and Generalitat de Catalunya grants 2017SGR1719 and 2017SGR696. Supported by ISCIII
38 (Instituto de Salud Carlos III, Spain), Project reference: 17-00134 cofinanced by FEDER Funds *A way to*
39 *make Europe*

40 **Keywords**

41 lipidomics; biomarkers; insulin resistance; preclinical models

42

43

44 **Abstract**

45 As obesity incidence is alarmingly rising among young individuals, we aimed to
46 characterize an experimental model of this situation, considering the similarity between
47 human and porcine physiology. For this reason, we fed prepubertal (63 days-old) Duroc
48 breed females (n=20) either with a standard growth diet (3800 KCal/day) or one with a
49 high-calorie content (5200 KCal/day) during 70 days. Computerized tomography, mass-
50 spectrometry based metabolomics, and lipidomics, as well as peripheral blood
51 mononuclear cell transcriptomics, were applied to define traits linked to high-calorie
52 intake. Samples from a human cohort confirmed potential lipidomic markers. Compared
53 to those fed a standard growth diet, pigs fed a high-calorie diet showed an increased
54 weight gain (13%), much higher adiposity (53%), hypertriacylglyceridemia and
55 hypercholesterolemia, in parallel to insulin resistance. This diet induced marked
56 changes in the circulating lipidome, particularly in phosphatidylethanolamine-type
57 molecules. Also, circulating specific diacylglycerol and monoacylglycerol contents
58 correlated with visceral fat and intrahepatic triacylglycerol concentrations. Specific lipids
59 associated with obesity in swine (mainly belonging to glycerophospholipid,
60 triacylglyceride, and sterol classes) were also linked with obesity-traits in the human
61 cohort, reinforcing the usefulness of the chosen approach. Interestingly, no overt
62 inflammation in plasma or adipose tissue was evident in this model. The presented model
63 is useful as a preclinical surrogate of prepubertal obesity in order to ascertain the
64 pathophysiology interactions between energy intake and obesity development.

65 **1. INTRODUCTION**

66 Childhood obesity is linked to severe metabolic derangements in adult life [1].
67 Epidemiological studies reveal alarming rates of incidence of prepubertal and pubertal
68 obesity [2], with its worrying impact on insulin resistance, development of type 2 diabetes,
69 increased cardiometabolic risk, decreased bone health, as well as the psychological
70 consequences of this derangement[3]. Therefore, the burden of increased caloric
71 unbalance could seriously affect pubertal and postpubertal health[1].

72

73 Obesity is considered a multifactorial situation [4]. Under an evolutionary point of view,
74 adipose tissue (AT) buildup in mammals can be a physiological response over changes
75 in calorie availability, with a signaling role [5,6], which could be useful for homeostasis in
76 an environment with energy availability oscillations. As such, increased fat content is not
77 always linked to metabolic derangements [7]. The continuum between these two
78 situations is still mostly unknown, leading to the uncertainty on why some individuals
79 develop insulin resistance and enhanced cardiometabolic risk even with lack of AT build-
80 up (metabolically unhealthy lean people) whereas other can cope with high amounts of
81 adipose tissue (metabolically healthy obese) [8]. It is required an adequate
82 characterization, at a molecular level, of the events between AT accumulation and its
83 consequences, to fill this gap of knowledge.

84

85 In this line, available experimental models of obesity show some intrinsic limitations. For
86 instance, rodents could exhibit increased obesity when placed in high-calorie intake,
87 especially in the so-called cafeteria diet (e.g., an unbalanced diet with high fructose or
88 high lipid content). Interestingly, due to the close physiological resemblance of porcine
89 and human physiologies, specific cardiometabolic markers translate better in pigs than
90 in rodent models. These include low HDL-cholesterol, increased LDL-cholesterol,
91 coronary calcification, to name a few. Thus, in both primates and swine, lipoprotein
92 metabolism is very similar to humans [9,10]. Therefore, unhealthy diets in these species
93 are able to induce changes in lipid profiles associated with cardiometabolic risk,
94 reproducing many changes present in humans [10,11]. Pigs are particularly suited for
95 evaluating their lipid metabolism, based on the knowledge of genetic traits controlling
96 them, and the possibility to monitor the buildup of AT by using clinical imaging systems
97 as computed tomography (CT)[12,13].

98

99 Systems biology has helped to unravel the pathogenic role of specific fat depots in both
100 humans and rodents. Among involved disciplines, proteomics, metabolomics, and
101 lipidomics are closely interlaced with the phenotype, offering a dynamic view of the
102 ongoing molecular changes. Metabolomics either focused on polar molecules or
103 lipidomics (when lipids are extracted before the analyses), have the advantage of
104 covering a high number of potential candidate biomarkers. When combined adequately
105 with confirmatory techniques, they could disclose pathogenic pathways amidst
106 generating novel hypotheses for diagnosis, prognosis, and therapeutics.

107

108 In this context, the present work aims to characterize molecular traits associated with the
109 obesity induced by a high-calorie diet in prepubertal female pigs. This goal is achieved
110 by combining an imaging platform based on CT evaluation of AT distribution, weight
111 evolution, food intake with changes in circulating lipidome and metabolome, with a view
112 of specific transcripts in the subcutaneous AT and in the transcriptome of the peripheral
113 blood mononuclear cells (PBMCs). These later were chosen as they may share, at least
114 partially, share the expression profile of different sets of genes with other tissues,
115 including those that reflect metabolic responses[14–16]. Furthermore, the lipidomic
116 changes were validated in a cohort of human subjects to confirm the robustness of these
117 observations. Finally, these changes were compared with clinically validated biomarkers
118 of obesity-related dyslipidemia with some of the suggested pathogenic pathways
119 confirmed in adipose and liver tissues.

120

121 **2. METHODS**

122 All the experimental procedures with pigs, including management, traits recording,
123 monitoring, and blood sampling, were approved by the Ethical Committee of the Institut
124 de Recerca i Tecnologia Agroalimentàries (IRTA, Girona, Spain). In the case of human
125 samples, these were obtained from the FLORINASH study cohort [17], and its
126 institutional review board approved the study protocol, and all subjects provided informed

127 written consent. Briefly, we recruited 44 consecutive subjects. Inclusion criteria were age
128 30–65 years and acceptance to study procedures. Exclusion criteria were a systemic
129 disease, infection in the previous month, chronic severe illness, ethanol intake >20 g/day,
130 or use of medications that might interfere with insulin action. For comparison with porcine
131 model-derived biomarkers, we recorded body to mass index (BMI) and homeostatic
132 model assessment for insulin resistance (HOMA-IR). See supplemental Table 1 for
133 clinical characteristics (supplemental data). Sources for chemicals are also presented in
134 the extended Methods section (supplemental data).

135 **2.1 Animals and treatments**

136 A total of 21 female piglets from a high intramuscular fat Duroc pig line were used in the
137 present study. Animals were born in 10 different litters (i.e., ten pairs of littermates) and
138 were distributed randomly to one of the two diets (conventional diet for growth and
139 western-type, see below). After weaning, piglets were transferred to the IRTA pig
140 experimental test station and subjected to the same management procedures. From
141 weeks 9 to 11, animals were adapted to a transition diet (Supplemental Tables 2 and 3).
142 Subsequently, each of the sibling pairs was divided into the two dietary treatments:
143 animals fed a conventional growth diet and animals fed a western-type diet with a high-
144 calorie, high-sucrose and low fiber content (detailed composition and nutritional
145 properties shown in supplemental Tables 4 and 5,). The experiment lasted until pigs
146 reached 19 weeks of age when animals were sacrificed after an overnight fast, at IRTA
147 experimental slaughterhouse compliance with all welfare regulations. Pigs were weighed
148 individually at the beginning and every two weeks during the whole experiment, plus the
149 day before slaughter. Daily feed intake (FI; kg/day) was recorded individually through
150 the automatic electronic feeding system HOKOFARM-IVO-G ® (Marknesse, The
151 Netherlands): all animals are identified electronically and located in contiguous pens in
152 the same barn (with 10 – 11 animal groups of littermates). Each pen is provided with an
153 automatic feeding recording system (system HOKOFARM-IVO-G ®), allowing full control

154 of individual voluntary *ad libitum* feed intake. Each particular meal intake (10 to 20 per
155 day) is recorded, and the full daily feed ingested amount is computed for each animal (as
156 well as the number and duration of meals). Blood samples for biochemical and
157 transcriptome analyses were taken from fasted animals immediately before sacrifice.
158 After slaughtering, pelvic-renal fat (flare fat) was removed and weighted.

159 **2.2 Computed tomography scanning and image analysis**

160 All pigs were CT-scanned one week before sacrifice employing the General Electric
161 HiSpeed ZX/I (Fairfield, CN, USA) equipment located at IRTA in Monells (Girona, Spain)
162 as explained in [12] and images were analyzed using software VisualPork [18,19]
163 developed by the University of Girona and IRTA. See Figure 1A and 1B as an example
164 of employed images. See the extended Methods section (supplemental data) for further
165 description.

166

167 **2.3 Biochemical analyses and western blot**

168 Serum lipids and other conventional biochemical variables were measured in fasted
169 animals in blood obtained immediately before sacrifice by using commercial kits,
170 including triacylglycerides, total cholesterol, LDL- cholesterol, HDL cholesterol, and
171 glucose, as described previously [20]. Plasma interleukin concentrations were measured
172 using Millipore multiplex kits for porcine samples (Millipore, Barcelona, Spain) according
173 to manufacturer instructions. Plasma insulin content was measured using a commercial
174 ELISA kit (Abcam, Cambridge, UK). Total lipids were extracted from the liver (80 mg)
175 and dried feces (100 mg) of the pigs and were quantified using the methods previously
176 described [21]. In the liver and feces samples, triglycerides and cholesterol were
177 quantified by colorimetric kits (QCA, Barcelona, Spain). Western blot analyses of tissues
178 were performed as described [20] and explained in the extended Methods section

179 (supplemental data), using as primary and secondary antibodies those listed in
180 supplemental Table 6 (supplemental data).

181 **2.4 Untargeted lipidomic analyses of plasma**

182 Plasma lipidomic analysis was based on a previously validated method [22]. Internal
183 standards (listed in supplemental Table 7), lipid extraction, and lipidomic techniques are
184 explained in the extended Methods section (supplemental data). Lipid extracts were
185 subjected to liquid chromatography coupled to mass spectrometry (LC-MS) using an
186 Agilent UPLC 1290 coupled to the Q-TOF MS/MS 6520 (Agilent Technologies,
187 Barcelona, Spain) based on a previously published method [23].

188 **2.5 Untargeted metabolomics analyses of serum**

189 The metabolomic analyses of serum extracts were performed by LC-MS and further
190 explained in the extended Methods section (supplemental data).

191 **2.6 Peripheral blood monocyte cells (PBMC) transcriptomics and AT leptin 192 expression**

193 PBMCs transcriptomics was done of (n=7 from each group) at the Centre for Omic
194 Sciences (Reus, Spain) by using the Porcine (V2) Gene Expression Microarray, 4x44K
195 (Agilent Technologies) following manufacturer's instructions. AT mRNA expression in
196 the subcutaneous depot was quantified as previously described [24] by using real-time
197 PCR in a LightCycler 480 Real-Time PCR System (Roche Diagnostics) using TaqMan®
198 technology suitable for relative gene expression quantification. Both methods are further
199 developed in the extended Methods section (supplemental data).

200 **2.7 Data processing, Network, and Statistic Analyses**

201 In the case of lipidomics and metabolomics, the MassHunter Data Analysis Software
202 (Agilent Technologies) was used to collect the results and the MassHunter Qualitative
203 Analysis Software (Agilent Technologies) to obtain the molecular features of the
204 samples, representing different, co-migrating ionic species of a given molecular entity
205 (i.e., ion adducts) using the Molecular Feature Extractor algorithm (Agilent Technologies)

206 [25]. This algorithm uses the accuracy of the mass measurements to group related ions
207 (based on the charge-state envelope, isotopic distribution, and the presence of different
208 adducts and dimers/trimers) assigning multiple species (ions) to a single compound
209 referred to as a feature. Finally, the MassHunter Mass Profiler Professional Software
210 (Agilent Technologies) was used to perform a non-targeted analysis over the extracted
211 features. Only shared features (found in at least 75% of the samples of the same
212 condition) were taken into account to correct for individual bias. In the case of non-
213 targeted lipidomics, proposed annotation by lipid class is based on exact mass, isotopic
214 distribution, and retention time of lipid family standards, so fatty acid distribution offered
215 is one of the potential combinations leading to the same number of carbons and
216 unsaturations.

217 In the case of non-targeted metabolomics, the identification of detected compounds with
218 significant differences was performed based on the exact mass, the adduct formation,
219 and the isotopes relative abundance and spacing using the Metlin/PCDL database and
220 Molecular Formula Generation software (Agilent Technologies).

221 In case of lipidomics, after log transformation and auto-scaling of variables, the masses
222 representing significant differences by Student's t-test ($p < 0.05$ with false discovery rate
223 correction) were searched against the LIPID MAPS database (The LIPID MAPS
224 Lipidomics Gateway, <http://www.lipidmaps.org/>, February 2018) (exact mass ppm < 20).
225

226 All other analyses were performed either with the SAS software ver. 9.4 (SAS Institute
227 Inc., Cary, NC, USA), with the Prism ver 7 (GraphPad Software, La Jolla, CA, USA) or
228 with the SPSS software ver 24 (IBM Corp, Armonk, NY, USA). Non-linear fit (exponential
229 growth equations; $Y=Y_0 \cdot \exp(k \cdot X)$) lines in the graphs correlating two variables were
230 produced with the Prism software. Multivariate statistics (Hierarchical Clustering, PCA,
231 and PLS-DA analyses) were done using the Metaboanalyst platform software [26]. Gene
232 enrichment and induced network module analyses were performed in the

233 ConsensusPathDB platform [27] using as input genes *agtpbp1*, *fcr14*, *herc4*, *egr2*,
234 *loc780435*, *loc100622399*, *loc100621244*, *krt18*, *ly49*, *pth*, *kctd14*, *ppp1r36*, and *trim46*.
235 The same list was also explored with the Genemania platform [28], using Homo sapiens
236 (human) as the reference and searching for its potential relationship with genes in lipid
237 metabolism *pemt* and *srbe1*.

238

239 **3. RESULTS**

240 As expected, animals under the western-type regime increased weight in a significant
241 amount (Table 1). However, despite these animals ingested near 37% more calories per
242 day, the difference in weight did not reach these changes, only achieving 13% more
243 weight. This ponderal change was also associated with an increased fecal fat content (in
244 cholesterol and triacylglyceride content). Nonetheless and despite these data pointing
245 for a trend for fecal lipid loss, adiposity, measured by CT imaging, increased sharply,
246 reaching *ca* two fold increases in AT derived parameters, such as relative fat volume and
247 pelvic-renal fat content. Concerning biochemical consequences associated with obesity,
248 animals under the high-calorie regime increased plasma cholesterol significantly, its
249 subfractions, and triacylglyceridemia in parallel to insulin resistance (HOMA-IR, *ca* 43%,
250 $p < 0.01$), suggesting an early impairment in glucose homeostasis (Table 1).

251

252 To enhance the knowledge of the molecular basis of this phenotype, we performed a
253 non-targeted lipidomic analysis in plasma samples. This approach shows that
254 prepubertal obesity changed the amounts of 187 molecules (p values ranging between
255 $1.49E-20$ and 0.05 ; Supplemental dataset 1), with very significant changes in 23
256 compounds (FDR < 0.1). These comprised 4 phosphatidylethanolamines and a
257 cerebroside, among the top markers. Hierarchical clustering resulted in a clear
258 separation between the two lipidomes using the 25 most statistically significant
259 molecules (Figure 1C) with a PLS-DA model (Figure 1D) with high accuracy (71%, with

260 R²=0.92 in a one model component, Supplemental Figure 1). Variable importance in
261 projection scores reinforced the importance of several phosphatidylethanolamine and
262 phosphatidylserine molecules in the first component, with a cerebroside, a
263 monoacylglycerol and a sterol related molecule among these discriminating features
264 (Supplemental Figure 1).

265

266 We studied if specific circulating lipids correlated with individual parameters affecting
267 final weight since the high-calorie intake impacted differently on each individual (e.g.,
268 variances higher than 10% in the final weight, Table 1). Concerning calorie consumption,
269 218 molecules correlated significantly with calorie intake (p values ranging between
270 7.61E-7 and 0.05, Spearman rank correlation between absolute values between 0.85
271 and 0.42, Supplemental Dataset 2). Among these, three phosphatidylethanolamines
272 were among the top targets correlating with calorie intake (Figure 1D). Interestingly,
273 several molecules also correlated with AT content (226 molecules, with p values
274 between 6.8 E-6 and 0.05, Spearman rank absolute correlation values between 0.81 and
275 0.43, Supplemental Dataset 3). Besides phosphatidylethanolamines, other lipids showed
276 a high correlation, such as a monoglyceride and a cerebroside (Figure 1E). The targets
277 correlating with pelvic-renal AT depot abundance were different from those of total fat,
278 suggesting the fact that non-subcutaneous fats constitute depots with unique
279 pathophysiological traits. Thus, 169 different molecules correlated with pelvic-renal
280 depot abundance (p values between 5.9E-5 and 0.05, Spearman rank absolute
281 correlation values between 0.76 and 0.43, Supplemental Dataset 4). Though
282 phosphatidylethanolamines were correlated as well, top molecules belonged to
283 cholesteryl esters and to phosphatidylserine (Figure 1F).

284

285 Interestingly and independently from lipidomic changes in plasma, a partial least square
286 discriminant analyses (PLS-DA) model encompassing AT depots and lipidemia variables
287 ((plasma, liver, and LDL cholesterol) exhibit a high accuracy (Supplemental Figure 2A).

288 Clustering analyses showed that not all the adipose tissue depots clusterized together,
289 with pelvic-renal fat being associated with lipidemia variables, (Supplemental Figure 2B).
290 In contrast, total fat and subcutaneous fat depot were more closely associated with
291 calorie intake and final weight. Variable importance in projection (Supplemental Figure
292 2C) showed that the most influential variables were calorie intake, total fat, and
293 subcutaneous fat percentages. Permutation tests demonstrated the robustness of this
294 model (Supplemental Figure 2D).

295

296 As LDL cholesterol was also affected by western-type regime, we evaluated potential
297 lipidomic markers linked to this biochemical trait. Interestingly, these differed from those
298 correlated with other biochemical characteristics. Thus, 165 molecules correlated with
299 LDL cholesterol concentrations (p values between 2.5×10^{-5} and 0.05, Spearman rank
300 correlation absolute values between 0.71 and 0.43, Supplemental Data Set 5). These
301 molecules comprised a specific phosphatidylethanolamine (different from the one
302 correlated with fat contents) and several unknown lipids (Supplemental Figure 3).

303

304 As increased fasting glycemia and HOMA-IR (despite no overt hyperinsulinemia) were
305 evidenced in this model of prepubertal obesity, we searched for lipidomic markers of
306 insulin resistance. Insulin concentrations were correlated with 90 different lipids (p values
307 between 0.0003 and 0.05, Spearman rank absolute correlation values between 0.68 and
308 0.43, Supplemental Dataset 6). Specific molecules comprised a phosphatidic acid and a
309 lactosyl-ceramide (Figure 2A). Similarly, a total of 77 molecules correlated with HOMA-
310 IR (p values between 0.0002 and 0.05, Spearman rank absolute correlation values
311 between 0.75 and 0.46, Supplemental Dataset 7). These included specific
312 triacylglycerides and sphingolipids (Figure 2A). Insulin acts on adipogenesis via specific
313 effectors such as SREBP1 [29]. Although we did not observe overt hyperinsulinism but
314 insulin resistance, we evaluated insulin-dependent signals in adipose tissues of this
315 model. The results demonstrate anatomic differences in the impact of a high-calorie diet

316 in insulin signaling modules of adipose tissue. Both adipose tissues from pelvic-renal
317 and omental locations showed a significantly increased amount of SREBP1c, while
318 subcutaneous and omental ATs locations showed decreased Glut4 levels, consistent
319 with insulin resistance (Figure 2B). Of note, AT in the pelvic-renal location did not show
320 detectable levels of Glut4 (data not shown), but Glut2. We also evaluated the expression
321 of specific mRNAs in the subcutaneous depot (Supplemental Table 8). We studied which
322 of the circulating lipids correlated with leptin expression since leptin levels mirror
323 adipogenesis in subcutaneous depot (significantly increased by evaluation of its mRNA
324 content in 186%, $p < 0.00001$). The results demonstrate significant associations of *leptin*
325 mRNA levels in subcutaneous AT and 138 lipids in plasma (p values between $4.92E-05$
326 and 0.049 , Spearman rank correlation absolute values between 0.76 and 0.43 ,
327 Supplemental Dataset 8). These include specific phosphatidylethanolamine and
328 triacylglycerides (Figure 2C). The specificity of the lipidomic changes associated with
329 insulin signaling is evidenced by the lack of common lipidomic correlations with leptin
330 mRNA and very low common correlations with fat content (Figure 2D).

331 As the liver is also a target of obesity, we evaluated the potential occurrence of hepatic
332 steatosis in this model. The results show that the western-type diet in this model did not
333 change neither triacylglycerides nor cholesterol content (Supplemental Figure 4).
334 Despite no significant changes were measured in phosphorylated-IRS1 (Ser 307, Ser
335 1101) or in phosphorylated c-Jun (Ser 73) (supplemental Figure 4) decreased Glut2
336 content potentially marked incipient insulin resistance, (Figure 3A), with some circulating
337 lipids correlating significantly with changes in hepatic fat content. Thus, 123 molecules
338 correlated with hepatic triacylglyceride content (p values between $1E-4$ and 0.05 ,
339 Spearman rank absolute correlation values between 0.74 and 0.43 , Supplemental
340 Dataset 9). These comprised a diacylglycerol and a phosphatidic acid (Figure 3B).
341 Plasma species correlating with liver triacylglyceride content are quite specific (Figure
342 3C). Noteworthy, changes in glucose transporters did not affect, at this stage, skeletal
343 muscle (Supplemental Figure 5).

344

345 In line with the moderate impact of high calorie in this model, plasma values of measured
346 interleukins did not demonstrate overt inflammation (Supplemental Table 9). However,
347 statistically significant correlations were present between circulating lipids and selected
348 interleukins, including IL-1a, IL-1b, and IL-18 (Supplemental figure 6, supplemental
349 Dataset 10 for correlated lipids). These lipids comprised specific
350 phosphatidylethanolamines, triacylglycerides, and tocopherol derivatives.

351

352 To evaluate whether this model could be of usefulness in human obesity, we compared
353 the results with those obtained from plasma lipidomic analyses of a human cohort. As
354 Figure 4 shows, there is a consistent overlap between the behavior of selected
355 biomarkers of obesity and its metabolic consequences between these two species. Thus,
356 selected phospholipid molecules (phosphatidylserine (21:0, 22:0), sterols (5-cholestan-
357 3-one), and unidentified lipids correlated significantly both with BMI in humans and with
358 fat abundance in pigs. Interestingly, other lipids also correlated with HOMA-IR in both
359 species, underlying the usefulness of the chosen model. The same behavior was
360 observed for correlations between cerebroside D, N-(11Z,14Z-eicosadienoyl)-
361 ethanolamine, TG (16:0/16:1(9Z)/16:1(9Z)) and BMI ($R^2=0.31$, $p<0.0001$; $R^2=0.09$,
362 $p<0.03$; $R^2=0.12$, $p<0.02$ after Pearson correlation analyses), as presented in
363 Supplemental Figure 7.

364

365 To further characterize the impact of western-type diet in the porcine model, we also
366 analyzed changes in the aqueous soluble phase of serum and explored changes in the
367 PBMC transcriptome profile. Globally speaking, the number of differential features was
368 much lower comparing the aqueous extracts with those of organic solvents
369 (Supplemental Table 8). When aggregating these changes of metabolites into pathways,
370 these defined a network that comprised variations in metabolites belonging to branched-
371 chain amino acids (BCAA), central carbon metabolism, and pantothenate and coenzyme

372 A synthesis (Figure 5). Changes in PBMC transcriptome (Supplemental Dataset 11),
373 when mapped, revealed two main networks affected by high-calorie intake
374 (Supplemental Figure 8). One was related to *EGR2*, and the other was mainly paired
375 with *KRT18* and *RAAR* genes. The functional annotation of these genes clustered in 4
376 different enriched neighborhood-based tests ($p < 0.001$), which included *SUV420H2*,
377 *DTX4*, *DTX1*, and *USP49* (Supplemental Figure 9). We also evaluated the potential
378 network proximity between genes in PBMC transcriptome and key genes in metabolism,
379 *SREBP1*, and *PEMT*. These two later belonged to the network of expression of *KRT18*
380 and *EGR2* (Supplemental figure 10).

381

382 **4. DISCUSSION**

383 The present work reinforces the usefulness of high-calorie regimes in porcine models to
384 evaluate obesity pathophysiology [30,31]. Interestingly, we found that the body weight
385 gain induced by high calorie, although significant, was not proportional to calorie intake.
386 This fits with the notion that weight gain and calorie intake are not linear[32]. In rats,
387 physical activity, among other factors, could divert dietary fats towards oxidation and less
388 to the storage, in a manner associated with de novo lipogenesis in adipose tissue, as
389 well as increases in skeletal muscle uptake and oxidation of lipids [33]. This metabolic
390 switch seems not uncommon in swine [34]. Of note, fat content increased in the high-
391 calorie group. In any case, our model can be viewed as an early obesity model, with
392 some traits of metabolic syndrome. This resemblance with human pathology has been
393 already described for domestic pigs under similar, high-fat regimes, where short term
394 interventions led to weight gain and dyslipidemia, but not tovert insulin resistance or
395 metabolic syndrome[35]. Several factors may explain the relatively small metabolic
396 impact in the current porcine model in comparison to other reported porcine models,
397 including the age of the individuals, the lack of a large amount of refined sugars (fructose
398 or sucrose), in comparison to other diets inducing obesity in porcine models, the specific
399 breed or the length of treatment.

400

401 In order to characterize the molecular traits explaining these obesity-related changes,
402 we performed non-targeted lipidomic analyses of plasma samples. For the sake of
403 brevity, we will limit mainly the discussion of those results obtained after FDR correction.
404 The results suggest the role of specific phosphatidylethanolamines as potential obesity
405 circulating biomarkers at a molecular level. One of the most differential identifiable
406 markers is a dimethylphosphatidylethanolamine. These products are intermediates in
407 the liver synthesis of phosphatidylcholine *de novo* biosynthesis through methylation of
408 phosphatidylethanolamine, especially relevant when choline is deficient in diet [36]. This
409 conversion is catalyzed by the enzyme phosphatidylethanolamine *N*-methyltransferase
410 (PEMT), whose activity is regulated by adenosylmethionine and
411 phosphatidylethanolamine levels. Since this activity is essential for VLDL secretion, we
412 hypothesize that increased levels of the dimethylphosphatidylethanolamine detected
413 could be a proxy for increased PEMT activity in the liver and VLDL secretion, required
414 for exporting hepatic lipids towards their adipose depot. PEMT loss renders protection
415 over diet-induced obesity[37], suggesting that in our model of obesity, this activity is
416 increased. Noteworthy, PEMT expression and colocalization are related with *EGR2* and
417 *KRT18*, as pathway analyses show. Other lipids significantly related to energy intake,
418 were specific phosphatidylethanolamine (PE) with long fatty acids. These findings could
419 go in line with data from lipidomic analyses of plasma from overweight and obese healthy
420 individuals [38]. In these analyses, other PE species appeared to be relevant
421 components of a plasma lipidomic signature of obesity. Interestingly, in other cohorts of
422 patients with prediabetes and diabetes, increased PE levels were noted as well [39]. In
423 this context, these were interpreted as a source for inflammatory eicosanoids, which may
424 be as well our case, as one of the potential fatty acids present in these PE is arachidonic
425 acid. Other works revealed an association of a specific PE, containing 40:6 fatty acids,
426 with insulin resistance in human individuals[40].

427

428 Reinforcing the validity of porcine lipid metabolism in the context of human obesity,
429 increases in specific PE-related species[41], such as plasmalogens, were observed in
430 obese subjects. Plasmalogens are part of an antioxidant response towards increased
431 oxidative stress with high-calorie intake. Nonetheless, several phospholipids
432 (phosphatidylserine and sterol molecules) correlated with BMI and AT abundance in
433 both species using the same methodological approach.

434

435 Other lipids were significantly associated with adiposity, measured by CT imaging. Thus,
436 increases in a long chain monoacylglycerol were detected. In mice, the deletion of one
437 of the enzymes linked to monoacylglycerol degradation, monoacylglycerol lipase, leads
438 to increased concentrations of monoacylglycerol and resistance to obesity, as well as
439 delayed lipid absorption [42]. The increased levels detected here may be viewed as a
440 potential homeostatic downregulation of monoacylglycerol lipase activity. Another lipid
441 showing a similar behavior with adiposity, cerebroside D, has been reported to be a
442 potent immunomodulatory agent in mice models of experimental colitis[43]. Furthermore,
443 glucocerebrosides afford protection over the metabolic syndrome induced by leptin loss
444 in mice [44]. It is known that structurally related compounds, such as glucosylated
445 ceramides and ceramides, play critical roles in insulin resistance, which has an
446 inflammatory background [45], therefore increased cerebroside D might be viewed as a
447 compensatory response to avoid the high-energy induced inflammatory burden. Of note,
448 cerebroside D was also found in the humane cohort used for the translational applicability
449 of the model, thereby reinforcing its potential importance in obesity pathophysiology.

450

451 In line with the pathophysiological relevance of the location of adipose tissue depots
452 [24], the lipids that correlated with total adiposity were different from those correlating
453 with the amount of pelvic-renal fat depot, a typical visceral location. Cholesteryl ester
454 18:3, associated with the amount of this AT, has been previously shown to be decreased
455 in a murine model of obesity [46]. However, and reinforcing the similarity of porcine

456 models with humans, a sizeable lipidomic survey revealed a significant association of
457 cholesteryl esters with body mass index in humans[47]. The other lipid, a
458 phosphatidylserine, has not been previously related to obesity, but instead to
459 preeclampsia in humans[48]. Glycerophosphoserines play vital structural roles in cell
460 membranes [49], where they may regulate oxidative stress responses and apoptosis,
461 but so far, it was not associated with high energy intake. Of note, a glycerophosphoserine
462 was found among the biomarkers shared between the porcine study and the humane
463 cohort. These lipids have been linked recently to changes in postprandial lipidome after
464 physical activity in humans with type 2 diabetes [50].

465

466 Finally, phosphatidic acid and diacylglycerol were associated with triacylglyceride
467 content in the liver. Interestingly, diacylglycerol species were as well noted as relevant
468 biomarkers by overfeeding experiments in humans[41], and phosphatidic acid increases
469 considerably during diet-induced nonalcoholic fatty liver disease [51]. Further, these data
470 reinforce the usefulness of plasma lipidomic signature for minimally invasive monitoring
471 of liver status [52].

472

473 Even though we detect no changes in some circulating surrogates of insulin resistance
474 (such as fructosamine), we were able to detect molecular markers of adipose tissue and
475 liver insulin resistance. Sphingolipids were found among the measured markers
476 correlating with HOMA-IR and insulin. This relationship agrees with the well-described
477 role of ceramide signaling in human obesity-related insulin resistance (reviewed in[53]).
478 Globally, this association would reinforce the validity of this model in evaluating the
479 pathophysiology of obesity-related metabolic rearrangements. In line with this, and
480 similar to humans, fat depots showed a location-specific response to high-calorie diet in
481 the expression of glucose transporters and adipogenic proteins (as SREBP-1c). Further,
482 AT leptin expression was increased, in line with adipose tissue expansion.

483

484 The changes in circulating metabolome and transcriptome also support the usefulness
485 of the model: changes in BCAA metabolism have been described in several clinical
486 studies, demonstrating that its alteration could predict diabetes development[54]. These
487 variations can be associated with ongoing inflammation and with mitochondrial
488 alterations, though in our model, no evidence for inflammation was found. Interestingly,
489 we also found pieces of evidence for altered pantothenic-related metabolic pathways in
490 our model of obesity. This concept fits with recently described findings in Yucatan mini-
491 pigs fed with a high-fat,high-sucrose diet for two months, also reporting amino acid
492 metabolism changes, reduced capacities of BCAA transamination, and alteration in
493 pantothenic metabolism [55]. In line with these results, transcriptomic changes in PBMC
494 agree with previous data in humans. Thus, previous data in adipocytes reveal that EGR
495 function, related to one of the pathways found in the transcriptome, is required to
496 enhance triacylglyceride depot [56]. In mice, EGR represses FOXC2 expression and is
497 required for the development of obesity under high-calorie intake. Of note, it is known
498 that insulin inhibits EGR expression in peripheral cells [57]. Therefore, one could see
499 EGR changes in PBMC as early markers for insulin dysfunction. Similarly, KRT18 has
500 been invoked as a biomarker for obesity-related hepatic dysfunction in obese
501 adolescents [58], so our finding of its change in this model would support its use as a
502 preclinical model of human pubertal obesity. Functional neighborhood analyses revealed
503 ubiquitin ligases DTX4 and DTX1 and the methyltransferase SUV420h2 as potential
504 nodes of interest, as previously reported data on adipocyte differentiation and diet-
505 induced obesity reveals [59,60]. These results reinforce the usefulness of PBMC
506 transcriptome analyses in this model.

507

508 We assume, as limitations of the present work, that only using a single-gender could
509 hinder the application of those results to human pathophysiology, especially those
510 related to the influence of sex hormones in lipid metabolism. However, the fact that many
511 markers were replicated in a completely independent fashion in a human cohort (with

512 both genders and older age) with obesity supports the usefulness of the chosen
513 approach. Further, we acknowledge that a more thorough examination of this cohort
514 (e.g., at older ages) would be advantageous to define the unique features of
515 prepubescent obesity in this context. Based on the comparative analyses with the human
516 cohort, we propose that those markers in common with consolidated obesity could show
517 some promise in the pathophysiological research of increased AT depots. In contrast,
518 those not in common with humans could be either derived from specific porcine
519 metabolism, from younger age of examined specimens, or related to resilience towards
520 pathological effects of AT buildup. Although the number of calories consumed is much
521 higher in comparison with humans (both in the conventional and in the western-type
522 diet), the experimental group exhibited a marked increase in daily intake of calories.
523 Further, on the qualitative side, experimental diets modeling western-type diets include
524 those such as the “cafeteria diet” with high-calorie content, high sucrose, and fat
525 contents, with lower protein amounts [61,62]). These also include high fat with high
526 cholesterol content[63]. Other authors also include a low fiber component[64]. Despite
527 this diversity, our model shows most of these traits, reproducing the western-type dietary
528 patterns. Further, lipidomic identification proposed aims at level 2, according to the
529 Metabolomics Standards Initiative [65], so they are putatively annotated compounds
530 (e.g., without chemical reference standards, based upon physicochemical properties and
531 spectral similarity with public/commercial spectral libraries). Therefore, some of these
532 reported metabolites might vary in their final identification., Noteworthy, our model of
533 prepubescent obesity may be useful for the evaluation of the biological basis of
534 metabolically healthy obesity. A high proportion of obese children are metabolically fit
535 [66]in a close relationship with a higher propensity of subcutaneous fat accumulation.
536 Our model shows both a high subcutaneous fat accumulation concurrently with a non-
537 marked inflammatory response. Further, some of the circulating lipids correlate with
538 physiological responses to AT expansion (e.g., leptin expression), while some others
539 correlate with pathological traits (inflammatory markers or the HOMA-IR). This fact

540 reveals the mixed nature of lipidomic responses to western-type diet in this model, but
541 we think that the reported data could be of interest in order to get the full profit of this
542 model as a *bona fide* preclinical surrogate of pubertal obesity.

543

544 **COMPETING INTERESTS**

545 No competing interests declared.

546 **FUNDING**

547 Supported by CDTI (Centro para el Desarrollo Tecnológico e Industrial, Spain), Project
548 reference: IPT-20111008, and Generalitat de Catalunya grants 2017SGR1719 and
549 2017SGR696. Supported by ISCIII (Instituto de Salud Carlos III, Spain), Project
550 reference: 17-00134 cofinanced by FEDER Funds *A way to make Europe*

551

552 **AUTHORS CONTRIBUTIONS**

553 Conceptualization: J.T., M.R.P., J.Pu., J.Pr., M.P.O.

554 Methodology: M.J., J.T., M.F.F., J.Pu., M.P.O.

555 Software: M.F.F., J.T., J.S., E.F.

556 Validation: R.B., L.A., M.M.G., J.M.F.R.

557 Formal analysis: M.J., J.C.E.S., J.S., A.Cr., A. Cast., M.S., F.J.O., L.A., J.M.F.R.

558 Investigation: M.J., J.C.E.S., A.C., H.R., A. Cr., R.R.M., A.Cast., M.S., R.Q.

559 Resources: M.R.P., J.T., R.Q., J.M.F.R.

560 Data curation: A.C., J.S., H.R., E.F.

561 Writing – original draft preparation: M.P.O., J.A.M., J.T.

562 Writing – review, and editing: R.Q., J.A.M., J. Pr, J.M.F.R., R.P., M.P.O

563 Visualization: R.P., M.F.F., E.F.

564 Project administration: J.T., M.R.P

565 Funding acquisition: J.T., M.R.P., J.M.F.R., M.P.O

566 **SUPPLEMENTARY DATA**

567 All supplementary figures and tables are present as supplementary information

568 available at Journal's website. Supplemental Datasets are freely available under
569 a CC BY 4.0 license at Figshare.com website at
570 <https://figshare.com/s/bf91f3332d1f6d9d4f26>

571

572 REFERENCES

- 573 [1] Liang Y, Hou D, Zhao X, Wang L, Hu Y, Liu J, et al. Childhood obesity affects
574 adult metabolic syndrome and diabetes. *Endocrine* 2015;50:87–92.
575 doi:10.1007/s12020-015-0560-7.
- 576 [2] Cunningham SA, Kramer MR, Narayan KMV. Incidence of childhood obesity in
577 the United States. *N Engl J Med* 2014;370:403–411.
578 doi:10.1056/NEJMoa1309753.
- 579 [3] Deckelbaum RJ, Williams CL. Childhood obesity: the health issue. *Obes Res*
580 2001;9 Suppl 4:239S–243S. doi:10.1038/oby.2001.125.
- 581 [4] Procter KL. The aetiology of childhood obesity: a review. *Nutr Res Rev*
582 2007;20:29–45. doi:10.1017/S0954422407746991.
- 583 [5] Trayhurn P, Beattie JH. Physiological role of adipose tissue: white adipose tissue
584 as an endocrine and secretory organ. *Proc Nutr Soc* 2001;60:329–339.
585 doi:10.1079/PNS200194.
- 586 [6] Trayhurn P, Bing C. Appetite and energy balance signals from adipocytes. *Philos*
587 *Trans R Soc Lond B, Biol Sci* 2006;361:1237–1249. doi:10.1098/rstb.2006.1859.
- 588 [7] Bervoets L, Massa G. Classification and clinical characterization of metabolically
589 “healthy” obese children and adolescents. *J Pediatr Endocrinol Metab*
590 2016;29:553–560. doi:10.1515/jpem-2015-0395.
- 591 [8] Phillips CM. Metabolically Healthy Obesity: Personalised and Public Health
592 Implications. *Trends Endocrinol Metab* 2016;27:189–191.
593 doi:10.1016/j.tem.2016.02.001.
- 594 [9] Litten-Brown JC, Corson AM, Clarke L. Porcine models for the metabolic
595 syndrome, digestive and bone disorders: a general overview. *Animal*
596 2010;4:899–920. doi:10.1017/S1751731110000200.
- 597 [10] Miller ER, Ullrey DE. The pig as a model for human nutrition. *Annu Rev Nutr*
598 1987;7:361–382. doi:10.1146/annurev.nu.07.070187.002045.
- 599 [11] Hamamdžić D, Wilensky RL. Porcine models of accelerated coronary
600 atherosclerosis: role of diabetes mellitus and hypercholesterolemia. *J Diabetes*
601 *Res* 2013;2013:761415. doi:10.1155/2013/761415.
- 602 [12] Carabús A, Gispert M, Brun A, Rodríguez P, Font-i-Furnols M. In vivo computed
603 tomography evaluation of the composition of the carcass and main cuts of
604 growing pigs of three commercial crossbreeds. *Livest Sci* 2014;170:181–192.
605 doi:10.1016/j.livsci.2014.10.005.
- 606 [13] Lucas D, Brun A, Gispert M, Carabús A, Soler J, Tibau J, et al. Relationship
607 between pig carcass characteristics measured in live pigs or carcasses with
608 Piglog, Fat-o-Meat'er and computed tomography. *Livest Sci* 2017;197:88–95.
609 doi:10.1016/j.livsci.2017.01.010.
- 610 [14] Reynés B, van Schothorst EM, Keijer J, Palou A, Oliver P. Effects of cold
611 exposure revealed by global transcriptomic analysis in ferret peripheral blood
612 mononuclear cells. *Sci Rep* 2019;9:19985. doi:10.1038/s41598-019-56354-6.
- 613 [15] Zeng Y, David J, Rémond D, Dardevet D, Savary-Auzeloux I, Polakof S.
614 Peripheral Blood Mononuclear Cell Metabolism Acutely Adapted to Postprandial
615 Transition and Mainly Reflected Metabolic Adipose Tissue Adaptations to a High-
616 Fat Diet in Minipigs. *Nutrients* 2018;10. doi:10.3390/nu10111816.

- 617 [16] Cifre M, Palou A, Oliver P. Cognitive impairment in metabolically-obese, normal-
618 weight rats: identification of early biomarkers in peripheral blood mononuclear
619 cells. *Mol Neurodegener* 2018;13:14. doi:10.1186/s13024-018-0246-8.
- 620 [17] Lelouvier B, Servant F, Païssé S, Brunet A-C, Benyahya S, Serino M, et al.
621 Changes in blood microbiota profiles associated with liver fibrosis in obese
622 patients: A pilot analysis. *Hepatology* 2016;64:2015–2027.
623 doi:10.1002/hep.28829.
- 624 [18] Boada I, Spinola J, Rodriguez J, Martínez R. VisualPork towards the simulation
625 of a virtual butcher. II Workshop on the Use Of ... 2009.
- 626 [19] Bardera A, Martínez R, Boada I, Font-i-Furnols M. VisualPork towards the
627 simulation of a virtual butcher. FAIM I Conference of COST ... 2012.
- 628 [20] Serrano JCE, Gonzalo-Benito H, Jové M, Fourcade S, Cassanyé A, Boada J, et
629 al. Dietary intake of green tea polyphenols regulates insulin sensitivity with an
630 increase in AMP-activated protein kinase α content and changes in mitochondrial
631 respiratory complexes. *Mol Nutr Food Res* 2013;57:459–470.
632 doi:10.1002/mnfr.201200513.
- 633 [21] Hara A, Radin NS. Lipid extraction of tissues with a low-toxicity solvent. *Anal*
634 *Biochem* 1978;90:420–426. doi:10.1016/0003-2697(78)90046-5.
- 635 [22] Pizarro C, Arenzana-Rámila I, Pérez-del-Notario N, Pérez-Matute P, González-
636 Sáiz J-M. Plasma lipidomic profiling method based on ultrasound extraction and
637 liquid chromatography mass spectrometry. *Anal Chem* 2013;85:12085–12092.
638 doi:10.1021/ac403181c.
- 639 [23] Castro-Perez JM, Kamphorst J, DeGroot J, Lafeber F, Goshawk J, Yu K, et al.
640 Comprehensive LC-MS E lipidomic analysis using a shotgun approach and its
641 application to biomarker detection and identification in osteoarthritis patients. *J*
642 *Proteome Res* 2010;9:2377–2389. doi:10.1021/pr901094j.
- 643 [24] Jové M, Moreno-Navarrete JM, Pamplona R, Ricart W, Portero-Otín M,
644 Fernández-Real JM. Human omental and subcutaneous adipose tissue exhibit
645 specific lipidomic signatures. *FASEB J* 2014;28:1071–1081. doi:10.1096/fj.13-
646 234419.
- 647 [25] Sana TR, Roark JC, Li X, Waddell K, Fischer SM. Molecular formula and
648 METLIN Personal Metabolite Database matching applied to the identification of
649 compounds generated by LC/TOF-MS. *J Biomol Tech* 2008;19:258–266.
- 650 [26] Xia J, Sinelnikov IV, Han B, Wishart DS. MetaboAnalyst 3.0--making
651 metabolomics more meaningful. *Nucleic Acids Res* 2015;43:W251–7.
652 doi:10.1093/nar/gkv380.
- 653 [27] Kamburov A, Pentchev K, Galicka H, Wierling C, Lehrach H, Herwig R.
654 ConsensusPathDB: toward a more complete picture of cell biology. *Nucleic Acids*
655 *Res* 2011;39:D712–7. doi:10.1093/nar/gkq1156.
- 656 [28] Warde-Farley D, Donaldson SL, Comes O, Zuberi K, Badrawi R, Chao P, et al.
657 The GeneMANIA prediction server: biological network integration for gene
658 prioritization and predicting gene function. *Nucleic Acids Res* 2010;38:W214–20.
659 doi:10.1093/nar/gkq537.
- 660 [29] White UA, Stephens JM. Transcriptional factors that promote formation of white
661 adipose tissue. *Mol Cell Endocrinol* 2010;318:10–14.
662 doi:10.1016/j.mce.2009.08.023.
- 663 [30] Spurlock ME, Gabler NK. The development of porcine models of obesity and the
664 metabolic syndrome. *J Nutr* 2008;138:397–402. doi:10.1093/jn/138.2.397.
- 665 [31] Pawar AS, Zhu X-Y, Eirin A, Tang H, Jordan KL, Woollard JR, et al. Adipose
666 tissue remodeling in a novel domestic porcine model of diet-induced obesity.
667 *Obesity (Silver Spring)* 2015;23:399–407. doi:10.1002/oby.20971.
- 668 [32] Hill JO, Wyatt HR, Peters JC. Energy balance and obesity. *Circulation*
669 2012;126:126–132. doi:10.1161/CIRCULATIONAHA.111.087213.
- 670 [33] Steig AJ, Jackman MR, Giles ED, Higgins JA, Johnson GC, Mahan C, et al.
671 Exercise reduces appetite and traffics excess nutrients away from energetically

- 672 efficient pathways of lipid deposition during the early stages of weight regain. *Am*
673 *J Physiol Regul Integr Comp Physiol* 2011;301:R656–67.
674 doi:10.1152/ajpregu.00212.2011.
- 675 [34] Zhang X, Lerman LO. The metabolic syndrome and chronic kidney disease.
676 *Transl Res* 2017;183:14–25. doi:10.1016/j.trsl.2016.12.004.
- 677 [35] Galili O, Versari D, Sattler KJ, Olson ML, Mannheim D, McConnell JP, et al.
678 Early experimental obesity is associated with coronary endothelial dysfunction
679 and oxidative stress. *Am J Physiol Heart Circ Physiol* 2007;292:H904–11.
680 doi:10.1152/ajpheart.00628.2006.
- 681 [36] Wu G, Zhang L, Li T, Zuniga A, Lopaschuk GD, Li L, et al. Choline
682 supplementation promotes hepatic insulin resistance in
683 phosphatidylethanolamine N-methyltransferase-deficient mice via increased
684 glucagon action. *J Biol Chem* 2013;288:837–847. doi:10.1074/jbc.M112.415117.
- 685 [37] Jacobs RL, Zhao Y, Koonen DPY, Sletten T, Su B, Lingrell S, et al. Impaired de
686 novo choline synthesis explains why phosphatidylethanolamine N-
687 methyltransferase-deficient mice are protected from diet-induced obesity. *J Biol*
688 *Chem* 2010;285:22403–22413. doi:10.1074/jbc.M110.108514.
- 689 [38] Holčapek M, Ovčačíková M, Lísa M, Cífková E, Hájek T. Continuous
690 comprehensive two-dimensional liquid chromatography-electrospray ionization
691 mass spectrometry of complex lipidomic samples. *Anal Bioanal Chem*
692 2015;407:5033–5043. doi:10.1007/s00216-015-8528-2.
- 693 [39] Meikle PJ, Wong G, Barlow CK, Weir JM, Greeve MA, MacIntosh GL, et al.
694 Plasma lipid profiling shows similar associations with prediabetes and type 2
695 diabetes. *PLoS One* 2013;8:e74341. doi:10.1371/journal.pone.0074341.
- 696 [40] Wallace M, Morris C, O'Grada CM, Ryan M, Dillon ET, Coleman E, et al.
697 Relationship between the lipidome, inflammatory markers and insulin resistance.
698 *Mol Biosyst* 2014;10:1586–1595. doi:10.1039/c3mb70529c.
- 699 [41] Heilbronn LK, Coster ACF, Campbell LV, Greenfield JR, Lange K, Christopher
700 MJ, et al. The effect of short-term overfeeding on serum lipids in healthy humans.
701 *Obesity (Silver Spring)* 2013;21:E649–59. doi:10.1002/oby.20508.
- 702 [42] Douglass JD, Zhou YX, Wu A, Zadrogra JA, Gajda AM, Lackey AI, et al. Global
703 deletion of MGL in mice delays lipid absorption and alters energy homeostasis
704 and diet-induced obesity. *J Lipid Res* 2015;56:1153–1171.
705 doi:10.1194/jlr.M058586.
- 706 [43] Wu X-F, Wu X-X, Guo W-J, Luo Q, Gu Y-H, Shen Y, et al. Cerebroside D, a
707 glycosphingolipid, improves experimental colitis in mice with multiple
708 targets against activated T lymphocytes. *Toxicol Appl Pharmacol* 2012;263:296–
709 302. doi:10.1016/j.taap.2012.07.001.
- 710 [44] Margalit M, Shalev Z, Pappo O, Sklair-Levy M, Alper R, Gomori M, et al.
711 Glucocerebroside ameliorates the metabolic syndrome in OB/OB mice. *J*
712 *Pharmacol Exp Ther* 2006;319:105–110. doi:10.1124/jpet.106.104950.
- 713 [45] Chavez JA, Summers SA. A ceramide-centric view of insulin resistance. *Cell*
714 *Metab* 2012;15:585–594. doi:10.1016/j.cmet.2012.04.002.
- 715 [46] Eisinger K, Liebisch G, Schmitz G, Aslanidis C, Krautbauer S, Buechler C.
716 Lipidomic analysis of serum from high fat diet induced obese mice. *Int J Mol Sci*
717 2014;15:2991–3002. doi:10.3390/ijms15022991.
- 718 [47] Weir JM, Wong G, Barlow CK, Greeve MA, Kowalczyk A, Almasy L, et al.
719 Plasma lipid profiling in a large population-based cohort. *J Lipid Res*
720 2013;54:2898–2908. doi:10.1194/jlr.P035808.
- 721 [48] Korkes HA, Sass N, Moron AF, Câmara NOS, Bonetti T, Cerdeira AS, et al.
722 Lipidomic assessment of plasma and placenta of women with early-onset
723 preeclampsia. *PLoS One* 2014;9:e110747. doi:10.1371/journal.pone.0110747.
- 724 [49] Leventis PA, Grinstein S. The distribution and function of phosphatidylserine in
725 cellular membranes. *Annu Rev Biophys* 2010;39:407–427.
726 doi:10.1146/annurev.biophys.093008.131234.

- 727 [50] Grace MS, Dempsey PC, Sethi P, Mundra PA, Mellett NA, Weir JM, et al.
728 Breaking up prolonged sitting alters the postprandial plasma lipidomic profile of
729 adults with type 2 diabetes. *J Clin Endocrinol Metab* 2017;102:1991–1999.
730 doi:10.1210/jc.2016-3926.
- 731 [51] Sanyal AJ, Pacana T. A Lipidomic Readout of Disease Progression in A Diet-
732 Induced Mouse Model of Nonalcoholic Fatty Liver Disease. *Trans Am Clin*
733 *Climatol Assoc* 2015;126:271–288.
- 734 [52] Gorden DL, Myers DS, Ivanova PT, Fahy E, Maurya MR, Gupta S, et al.
735 Biomarkers of NAFLD progression: a lipidomics approach to an epidemic. *J Lipid*
736 *Res* 2015;56:722–736. doi:10.1194/jlr.P056002.
- 737 [53] Aburasayn H, Al Batran R, Ussher JR. Targeting ceramide metabolism in
738 obesity. *Am J Physiol Endocrinol Metab* 2016;311:E423–35.
739 doi:10.1152/ajpendo.00133.2016.
- 740 [54] Giesbertz P, Daniel H. Branched-chain amino acids as biomarkers in diabetes.
741 *Curr Opin Clin Nutr Metab Care* 2016;19:48–54.
742 doi:10.1097/MCO.0000000000000235.
- 743 [55] Polakof S, Dardevet D, Lyan B, Mosoni L, Gatineau E, Martin J-F, et al. Time
744 Course of Molecular and Metabolic Events in the Development of Insulin
745 Resistance in Fructose-Fed Rats. *J Proteome Res* 2016;15:1862–1874.
746 doi:10.1021/acs.jproteome.6b00043.
- 747 [56] Zhang J, Zhang Y, Sun T, Guo F, Huang S, Chandalia M, et al. Dietary obesity-
748 induced Egr-1 in adipocytes facilitates energy storage via suppression of FOXC2.
749 *Sci Rep* 2013;3:1476. doi:10.1038/srep01476.
- 750 [57] Aljada A, Ghanim H, Mohanty P, Kapur N, Dandona P. Insulin inhibits the pro-
751 inflammatory transcription factor early growth response gene-1 (Egr)-1
752 expression in mononuclear cells (MNC) and reduces plasma tissue factor (TF)
753 and plasminogen activator inhibitor-1 (PAI-1) concentrations. *J Clin Endocrinol*
754 *Metab* 2002;87:1419–1422. doi:10.1210/jcem.87.3.8462.
- 755 [58] Giannini C, Feldstein AE, Santoro N, Kim G, Kursawe R, Pierpont B, et al.
756 Circulating levels of FGF-21 in obese youth: associations with liver fat content
757 and markers of liver damage. *J Clin Endocrinol Metab* 2013;98:2993–3000.
758 doi:10.1210/jc.2013-1250.
- 759 [59] Liu P, Hsieh P, Lin H, Liu T, Wu H, Chen C, et al. Grail is involved in adipocyte
760 differentiation and diet-induced obesity. *Cell Death Dis* 2018;9:525.
761 doi:10.1038/s41419-018-0596-8.
- 762 [60] Son MJ, Kim WK, Oh K-J, Park A, Lee DS, Han BS, et al. Methyltransferase and
763 demethylase profiling studies during brown adipocyte differentiation. *BMB Rep*
764 2016;49:388–393. doi:10.5483/BMBRep.2016.49.7.062.
- 765 [61] Wright TM, King MV, Davey WG, Langley-Evans SC, Voigt J-PW. Impact of
766 cafeteria feeding during lactation in the rat on novel object discrimination in the
767 offspring. *Br J Nutr* 2014;112:1–5. doi:10.1017/S0007114514003134.
- 768 [62] Krawczyńska A, Herman AP, Antushevich H, Bochenek J, Dziendzikowska K,
769 Gajewska A, et al. Modifications of Western-type diet regarding protein, fat and
770 sucrose levels as modulators of steroid metabolism and activity in liver. *J Steroid*
771 *Biochem Mol Biol* 2017;165:331–341. doi:10.1016/j.jsbmb.2016.07.012.
- 772 [63] Sari G, Meester EJ, van der Zee LC, Wouters K, van Lennep JR,
773 Peppelenbosch M, et al. A mouse model of humanized liver shows a human-like
774 lipid profile, but does not form atherosclerotic plaque after western type diet.
775 *Biochem Biophys Res Commun* 2020. doi:10.1016/j.bbrc.2020.01.067.
- 776 [64] Statovci D, Aguilera M, MacSharry J, Melgar S. The impact of western diet and
777 nutrients on the microbiota and immune response at mucosal interfaces. *Front*
778 *Immunol* 2017;8:838. doi:10.3389/fimmu.2017.00838.
- 779 [65] Sumner LW, Amberg A, Barrett D, Beale MH, Beger R, Daykin CA, et al.
780 Proposed minimum reporting standards for chemical analysis *Chemical Analysis*

781 Working Group (CAWG) Metabolomics Standards Initiative (MSI). *Metabolomics*
782 2007;3:211–221. doi:10.1007/s11306-007-0082-2.
783 [66] Vukovic R, Dos Santos TJ, Ybarra M, Atar M. Children with metabolically healthy
784 obesity: A review. *Front Endocrinol (Lausanne)* 2019;10:865.
785 doi:10.3389/fendo.2019.00865.
786
787

788 **FIGURE LEGENDS**

789

790 **Figure 1. A western-type diet induces prepubertal obesity, and it defines a specific**

791 **lipidomic signature in plasma.** A) Representative CT images of the porcine model of prepuberal

792 obesity showing accumulation of AT in animals under a western-type diet. B) Example of

793 determination of subcutaneous fat (red), intermuscular fat (green), and flare fat, including pelvic-

794 renal depot (orange) from CT images. C) Hierarchical clustering and heatmap shows a plasma

795 lipidomic signature of high-calorie (western-type diet) in the porcine model. In the right panel, the

796 PLS-DA model using plasma lipidomics demonstrates high accuracy (>65%, $R^2=0.99$) in

797 classification. Selected lipids are significantly associated with individual calorie intake (D), global

798 fat abundance (E), and pelvic-renal fat abundance (F) as measured by CT in vivo. Shown lipids

799 are a selection from those showing a significant correlation with specific traits (at least $p<0.05$ by

800 Spearman's rank correlation test, lines indicate non-linear fit (exponential growth equations;

801 $Y=Y_0 \cdot \exp(k \cdot X)$). see Supplemental Data for the whole list).

802

803 **Figure 2. The prepubescent obesity model described induces changes in circulating**

804 **insulin levels and its action, in association with specific plasma lipids and with changes**

805 **in AT insulin-regulated proteins.** Association of plasma concentration of selected lipids with

806 individual insulin concentrations and HOMA-IR values (A). B shows a representative western-blot

807 of insulin-responsive signals in AT and the influence of western-type diet. Right graphs after each

808 blot show densitometric integrated values normalized to the intensity of animals fed with

809 conventional diets all adjusted to total protein content, estimated by Coomassie blue staining,

810 with p values after Student's t-test. Considering all values from each protein, with a two way

811 ANOVA significant differences were found as well for Glut2 in the subcutaneous depot, and for

812 SREBP1 in omental and pelvic-renal depots ($p<0.05$, $p<0.01$ and $p<0.02$ respectively by post hoc

813 analyses, n ranging 3 to 9 different samples). C) Subcutaneous adipose tissue leptin mRNA levels

814 are associated with specific circulating lipids. D) Venn diagram showing the specificity of

815 correlations, based on the very low (or absent) overlap between circulating lipids associated (at

816 least $p<0.05$ by Spearman's rank correlation test) with HOMA-IR, with subcutaneous adipose

817 tissue leptin mRNA, and with fat content. Shown lipids in A and C are a selection from those

818 showing significant correlation with these specific traits (at least $p<0.05$ by Spearman's rank

819 correlation test, lines indicate non-linear fit (exponential growth equations; $Y=Y_0 \cdot \exp(k \cdot X)$, see
820 Supplemental Data for the whole list)

821

822 **Figure 3. Liver insulin-responsive signals and relationship with circulating lipidome.** A)

823 Representative western-blot of insulin-responsive signals in the liver with * in Glut 2 indicating
824 differences induced by western-type diet ($p < 0.05$ by Student's t-test). B) Liver triacylglyceride

825 (TAG) levels are associated with specific circulating lipids. C) Venn diagram showing the

826 specificity of correlations, based on the very low (or absent) overlap between circulating lipids

827 associated (at least $p < 0.05$ by Spearman's rank correlation test) with hepatic TAG levels, with

828 HOMA-IR, with subcutaneous adipose tissue leptin mRNA and with fat content. Shown lipids in

829 B are a selection from those showing significant correlation with specific traits (at least $p < 0.05$ by

830 Spearman's rank correlation test, lines indicate non-linear fit (exponential growth equations;

831 $Y=Y_0 \cdot \exp(k \cdot X)$), see Supplemental Data for the whole list)

832

833 **Figure 4. Validation in humans with obesity of proposed biomarkers.** Specific lipids show a

834 similar positive correlation with BMI (in humans, in B, D, and F) and AT abundance (in the porcine

835 model, in A, C, and E). The same is presented for HOMA-IR correlations (for pigs in G and

836 humans in H). All correlations are significant (at least $p < 0.05$) by Spearman's rank correlation

837 test. Lines indicate non-linear fit (exponential growth equations; $Y=Y_0 \cdot \exp(k \cdot X)$). Pig icon comes

838 from aLf; and Human one by Ma Qing both from the Noun Project (thenounproject.com)

839

840 **Figure 5. Interactomics of plasma metabolites associated with a western-type diet.**

841 Metabolites were mapped to a pathway database (in this case, KEGG), and nodes, representing

842 pathways (identified by pathway name in the database), is proportional to the number of

843 metabolites contained in the pathway. Node color intensity is associated with the hypergeometric

844 test accounting number of metabolites associated with high-calorie diet and those potentially

845 present in the specific pathway (node), while edge width represents the percentage of shared

846 metabolites between pathways and edge color indicate the number of metabolites associated

847 with western-type diet.

848

849

Table 1. Morphological, calorie consumption and biochemical traits

Parameter	Conventional diet	Western-type diet	p ¹
Initial weight (Kg)	16.5±2.8	16.7±2.2	0.86
Final weight (Kg)	53.2±5.7	60±8.36	0.043
Weight gain (Kg/d)	0.58±0.06	0.68±0.1	0.024
Caloric consumption (Kcal/d)	3819.7±236.5	5213.9±516.8	<0.0001
Fecal fat content (mg/g)	19.5±1.3	50±8	0.02
Pelvic-renal fat weight (Kg)	0.188±0.026	0.405±0.082	0.008
Relative fat volume at VL2 (%)	12.7±1.2	19.4±2.6	0.002
Blood Cholesterol (mg/dL)	125.9±24.4	155.7±26.4	0.015
Blood LDL-Cholesterol (mg/dL)	46.8±8.1	57.1±8.5	0.011
Blood HDL-Cholesterol (mg/dL)	45.2±9.9	61.3±13.8	0.007
Triacylglyceridemia (mg/dL)	21.6±6.3	29.2±5.9	0.014
Glycemia (mg/dL)	80.75±16.73	108.6±23.9	0.01
Fructosamine (mg/dL)	177.6±24.9	152.1±46.8	0.131
Insulinemia (pg/mL)	5.65±0.24	5.77±0.46	0.26
HOMA-IR	1.09±0.21	1.56±0.39	0.009

850
851
852

Values shown are mean±SD, unless stated otherwise. ¹Student's t test comparison between values in conventional and western-type diets

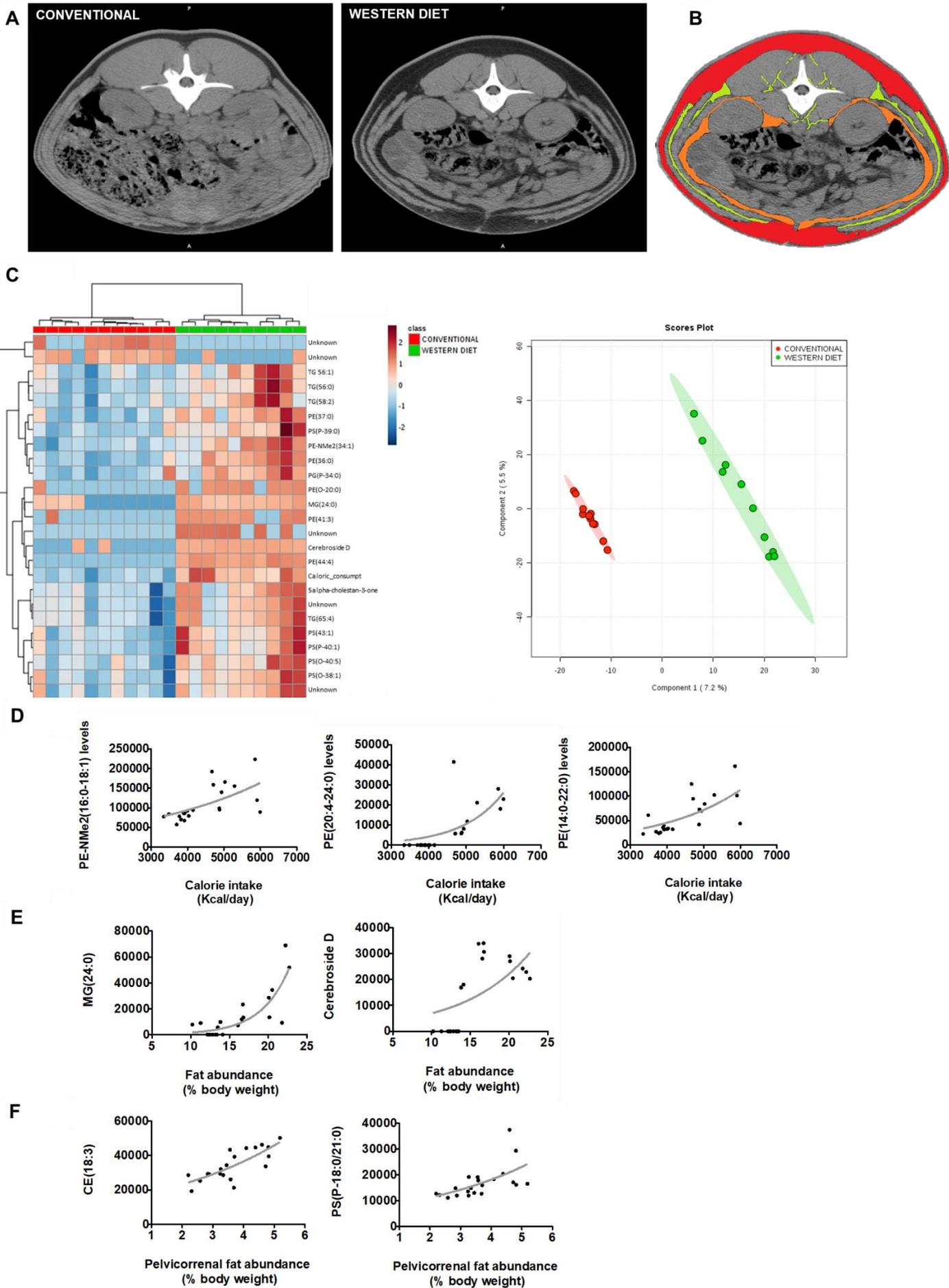
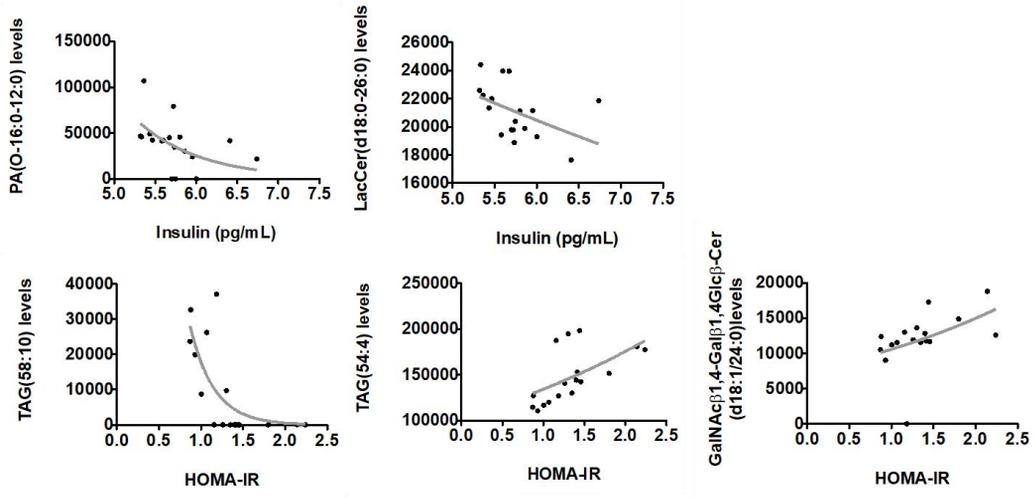
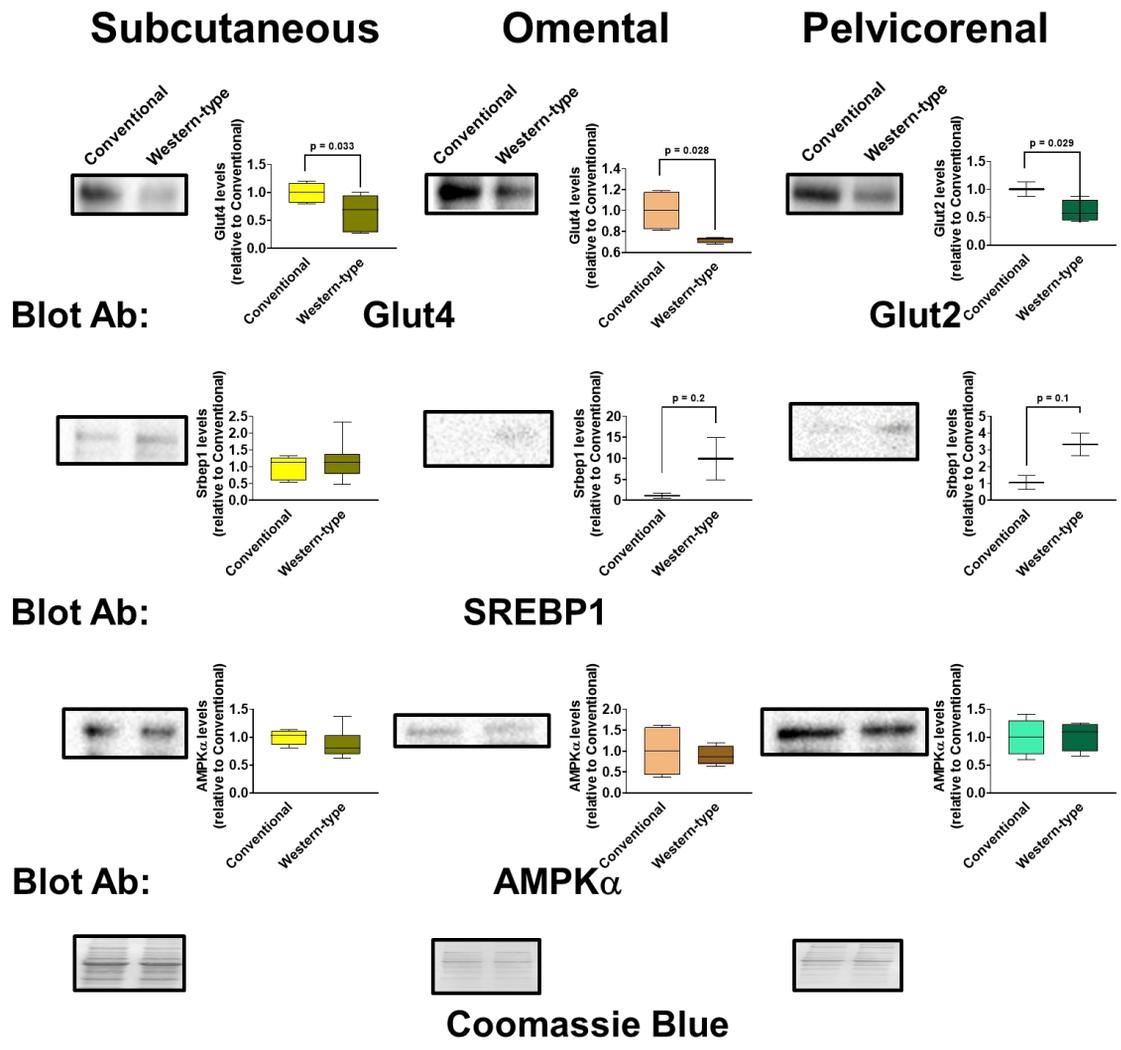
FIGURE 1

FIGURE 2

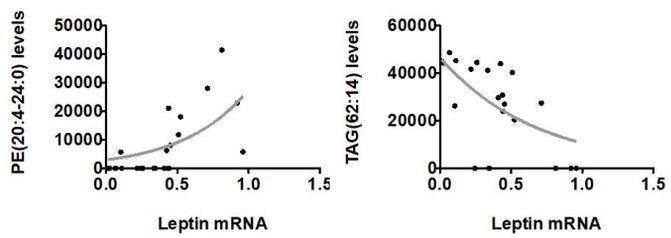
A



B



C



D

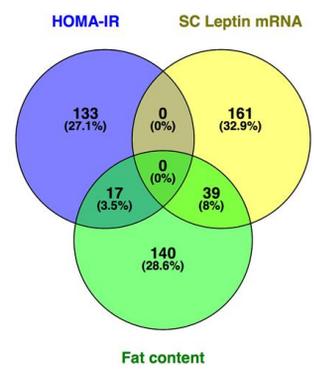
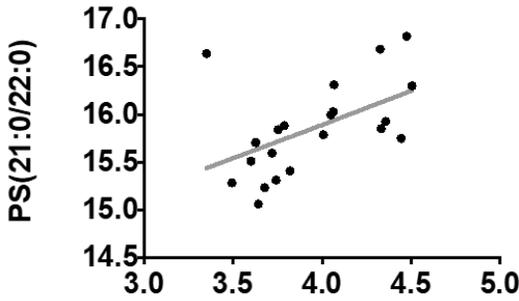


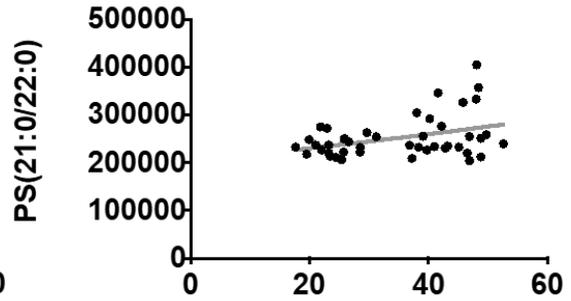
FIGURE 4



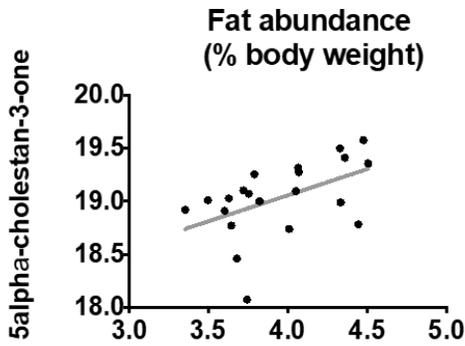
A



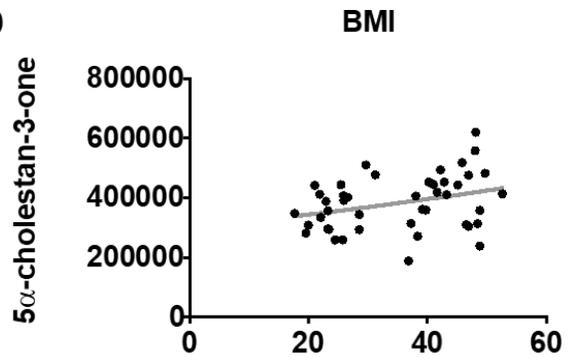
B



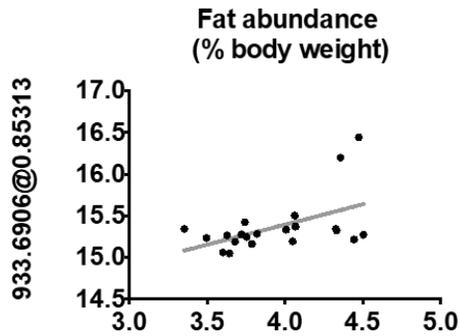
C



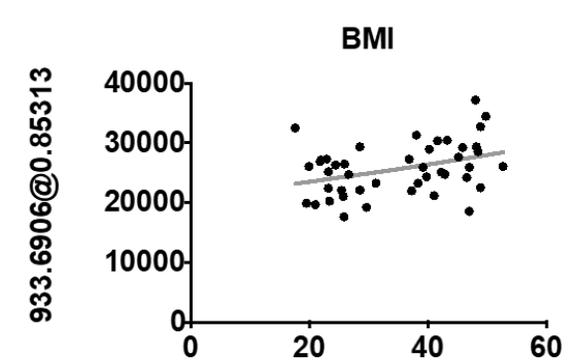
D



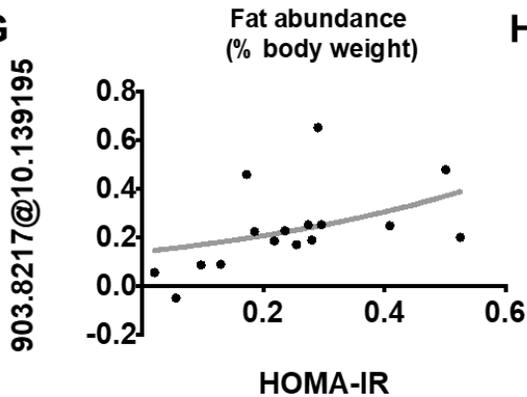
E



F



G



H

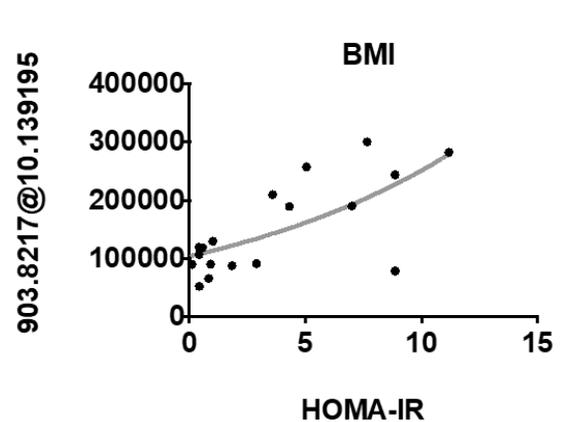
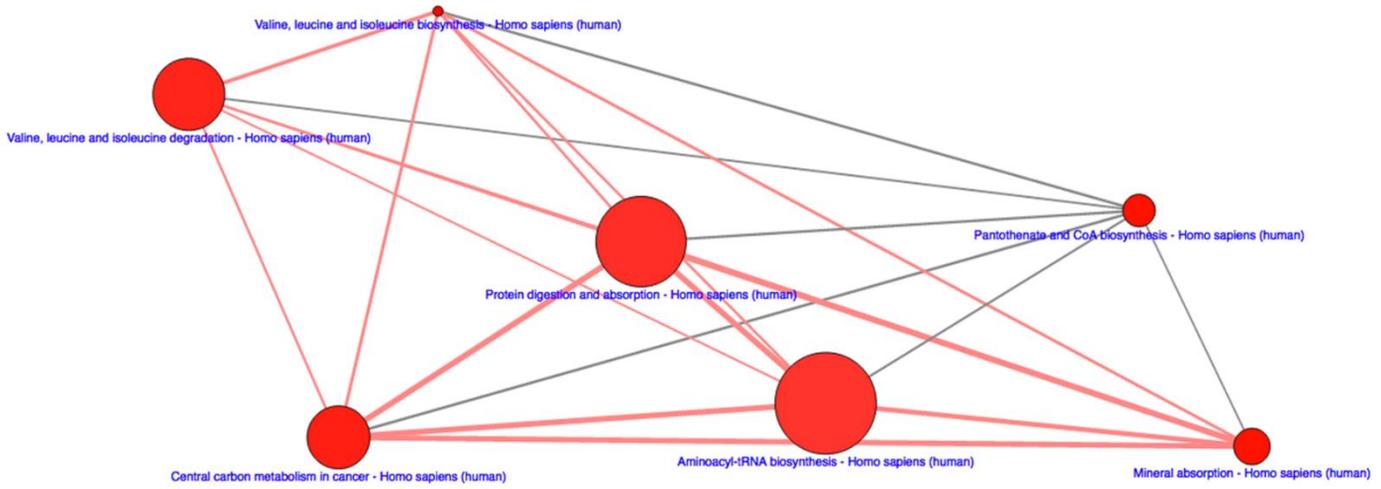


FIGURE 5



Node size (# metabolites)	Node color (p value)	Edge width (% shared metabolites)	Edge color (metabolites from input)
23 metabolites	$p < 10^{-1}$	1%	1
34 metabolites	$p < 10^{-0}$	50%	0
52 metabolites	$p = 1.0$	100%	0

1 **EXTENDED METHODS**

2 **Chemicals**

3 For lipidomic analyses and other analytical procedures, synthetic lipids were obtained from
4 Avanti Polar Lipids Inc. (Alabaster, AL, USA) and Sigma-Aldrich (Madrid, Spain). Methyl tert-
5 butyl ether (MTBE), acetonitrile, potassium chloride, chloroform, ammonium formate and
6 ammonium hydroxide -all liquid chromatography-mass spectrometry (LC-MS) grade- were
7 purchased from Sigma-Aldrich (Madrid, Spain); methanol was from Carlo Erba (Milano, Italy);
8 acetone was from Riedel-de-Häen (Seelze, Germany); and LC/MS-grade isopropanol and
9 formic acid were from Baker (Phillipsburg, NJ, USA).

10

11 **Computed tomography scanning and image analysis**

12 Previously to the scan, animals were fasted for 16 h and anesthetized with azaperone (0.1
13 mg/kg body weight (BW)), ketamine (0.2 mg/kg BW), and, if necessary, propofol (0.22 mg/kg
14 BW) as explained in [1]. Pigs were scanned in the prone position, and acquisition parameters
15 were axial, 1 s, 140 kV, 145 mA, 5 mm thickness, matrix 512x512, and displayed field of view
16 adapted to the size of each pig. Scanning lasted approximately 20 min per pig. For each pig,
17 one axial image was obtained at the level of the 2nd lumbar vertebrae (2VL).

18 Images were analyzed with the software VisualPork [2,3] developed by the University of
19 Girona and IRTA. Image analysis was those explained in ValLaillet *et al.* [4] modified. Thus,
20 the mean and standard deviation of the Hounsfield (HU) value of the subcutaneous fat were
21 obtained from each image. These values were used for the determination of the fat tissue
22 content. From each image, an ROI (region of interest) was determined that considered all the
23 outlines of the pig (ROI1), *i.e.*, the total area of the image. Another area was taken at for the
24 interior part of the subcutaneous fat of each image (ROI2), which corresponds to the area of
25 the image, excluding subcutaneous fat and skin. Another area was obtained, including all the
26 intraabdominal region, being the ribs, and the tenderloin the borders (ROI3). Finally,
27 intraperitoneal area, going through the junction between flare fat and internal organs (ROI4),

28 was determined. For each ROI (from ROI1 to ROI4), the AT area was calculated, considering
29 the range of HU values between the mean HU value plus/minus two standard deviations
30 previously determined. These areas were transformed into mm³, considering the DFOV, the
31 matrix size, and the thickness [5]. From the volume of ROI1 minus those from ROI2, the
32 subcutaneous fat was obtained. Intermuscular fat was obtained as the fat volume in ROI2
33 minus ROI3 and flare fat as the fat volume of ROI3 minus those of ROI4. The ratio between
34 the volume of the total fat (subcutaneous, intermuscular, and flare fat) and the total volume of
35 the image was determined and converted into a percentage (relative fat volume at VL2).

36

37 Samples were homogenized in a buffer containing 180 mM KCl, five mM MOPS, two mM
38 EDTA, one mM diethylenetriaminepentaacetic acid, and one μM butylated hydroxyl toluene,
39 10 μg/ml aprotinin, one mM NaF, one mM Na₃VO₄ and a protease inhibitor mix (GE
40 Healthcare 80-6501-23, USA) (1% v/v) with a Potter-Elvehjem device, at 4 °C. After brief
41 centrifugation (500 × g, 5 min) protein concentrations were measured in the supernatants
42 using the Bradford protein assay (BioRad Laboratories, München, Germany). Tissue protein
43 (15-40 mg) was resolved by SDS-PAGE and electroblotted onto polyvinylidene difluoride
44 membranes (Immobilon-P, Millipore, Bedford, USA). Immunodetection was performed using
45 as primary and secondary antibodies, those listed in Supplemental Table 6. A monoclonal
46 antibody to β-actin (Sigma, USA) and Coomassie blue staining were used to control protein
47 loading. Protein bands were visualized with the chemiluminescence ECL method (Millipore
48 Corporation, Billerica, MA, USA). Luminescence was recorded and quantified in Lumi-Imager
49 equipment from Boehringer (Mannheim, Germany), using the Quantity One 4.6.5. Software.

50 **Lipidomic analyses**

51 ***Preparation of Lipid Standards*** Lipid standards consisting of isotopically labeled lipids (see
52 Supplemental Table 7) were used for external standardization (i.e., lipid family assignment)
53 and internal standardization (i.e., for adjustment of potential inter- and intra-assay variances).
54 Stock solutions were prepared by dissolving lipid standards in MTBE at a concentration of
55 1mg/mL, and working solutions were diluted to 2.5μg/mL in MTBE.

56 **Lipid extraction** Briefly, in order to precipitate plasma protein fraction, 5µl of Mili Q water and
57 20µl of methanol were added to 10µl of a plasma sample. After the addition, samples were
58 vigorously shaken for 2 min. Then, for lipid extraction, 250µl of MTBE (containing internal lipid
59 standards) were added, and samples were immersed in a water bath (ATU Ultrasonidos,
60 Valencia, Spain) with an ultrasound frequency and power of 40kHz and 100W, respectively,
61 at 10°C for 30 min. Then, 75 µL of Mili Q water was added to the mixture, and the organic
62 phase was separated by centrifugation (1,400 x g) at 10 °C for 10 min. Lipid extracts contained
63 in the upper phase were collected and subjected to mass spectrometry. A pool of all lipid
64 extracts was prepared and used as quality controls, as previously described [6].

65

66 **LC-MS/MS method** Sample compartment was refrigerated at 4°C, and for each sample, 10µl
67 of lipid extract was applied onto 1.8 µm particle 100 x 2.1 mm id Waters Acquity HSS T3
68 column (Waters, Milford, MA, USA) heated to 55°C. The flow rate was 400µl/min with solvent
69 A composed of 10mM ammonium acetate in acetonitrile-water (40:60, v/v) and solvent B
70 composed of 10mM ammonium acetate in acetonitrile-isopropanol (10:90, v/v). The gradient
71 started at 40% B and reached 100% B in 10min and held for 2 min. Finally, the system was
72 switched back to 60% B and equilibrated for 3min. Duplicate runs of the samples were
73 performed to collect positive and negative electrospray ionized lipid species in a TOF mode,
74 operated in full-scan mode at 100 to 3000m/z in an extended dynamic range (2 GHz), using
75 N₂ as nebulizer gas (5L/min, 350°C). The capillary voltage was set 3500 V with a scan rate of
76 1scan/s. Continuous infusion using a double spray with masses 121.050873, 922.009798
77 (positive ion mode), and 119.036320, 966.000725 (negative ion mode) was used for in-run
78 calibration of the mass spectrometer.

79 **Untargeted metabolomics analyses of serum**

80 For extraction of metabolites, 1.8ml of a methanol/water 8:1 (v/v) was added to 200 µl of serum
81 sample. After stirring for 1 min and centrifugation (1400 x g) for 10 min at 4°C, the supernatant
82 with water-soluble metabolites was placed into a new vial, and the pellet was washed twice

83 with additional methanol/water. The combined upper-phases solutions were partially dried
84 under N₂ flow until methanol removal. Finally, the solution was quickly frozen and lyophilized.

85

86 The LC-MS analysis of aqueous serum extract samples was done using a Q-TOF/MS 6550
87 mass spectrometer (Agilent Technologies) with an Agilent UPLC 1290 chromatographic
88 system. The lyophilized samples were reconstituted by adding 200 µl of 0.1% formic acid in
89 water and injected onto a 1.8 µm particle 50 x 2.1 mm id Zorbax SB-Aq RR column (Agilent
90 Technologies) which was heated to 60°C in the column oven. A binary gradient system
91 consisting of 0.2% acetic acid in water (solvent A) and 0.2% acetic acid in methanol (solvent
92 B) was used. The flow rate was 0.5 mL/min, and the solvent gradient program was 0 to 1 min
93 2% B isocratic, 1 to 13 min 98% B, 13 to 19 min 98% B isocratic, 1 min 0% B, and then
94 equilibrated for an additional 5 min. The autosampler temperature was maintained at 4°C, and
95 the injection volume was 10 µl.

96 Ionization was performed in an electrospray source mode, with a drying gas temperature and
97 a flow of 150°C and 14 mL/min, respectively; a sheath gas temperature and flow of 300°C and
98 11 mL/min, respectively; a nebulizer pressure of 30 psi; a capillary voltage of 3,000 V; and a
99 nozzle voltage of 500 V. QTOF was operated in MS Full Scan mode in positive polarity,
100 applying a fragmentary voltage of 380 V, an acquisition rate of 5 spectra/s and an acquisition
101 range from 50 to 1700 m/z. Blank samples and quality control samples were injected regularly
102 between the runs to ensure the quality of the data.

103 **Peripheral blood monocyte cells (PBMC) and AT transcriptomics**

104 Briefly, PBMCs were isolated from animal blood by Ficoll gradient separation (GE Healthcare,
105 Piscataway, NJ, USA) and PBMC total RNA was extracted using Tripure Reagent (Roche
106 Diagnostic, Barcelona, Spain) and purified with Qiagen RNeasy Mini Kit spin columns (Izasa,
107 Barcelona, Spain). Blood samples (10 mL) were diluted (1:1) with phosphate buffer saline (pH:
108 7.4), and PBMC were isolated by Ficoll gradient separation, according to the instructions
109 indicated by the manufacturer (GE Healthcare Bio Sciences). The PBMC pellet was carefully

110 resuspended with 4 mL of erythrocyte lysis buffer (155 mM NH₄Cl, ten mM KHCO₃, and 100
111 μM EDTA, pH: 7.4), incubated at room temperature for 5 minutes and centrifuged at 400 g for
112 10 minutes. Finally, the supernatant was aspirated, and the PBMC pellet was stored at -70°C
113 until RNA analysis. PBMC total RNA was extracted using Tripure Reagent (Roche Diagnostic)
114 and purified with Qiagen RNeasy Mini Kit spin columns (Izasa). RNA quantity was measured
115 spectrophotometrically (NanoDrop®), and RNA quality was confirmed with the Agilent 2100
116 Bioanalyzer (Agilent Technologies).

117

118 The gene expression levels were assessed using Porcine (V2) Gene Expression Microarray,
119 4x44K (Agilent Technologies) following the manufacturer's instructions. This microarray
120 quantifies 43,603 probe sets. Labeling and hybridization of the samples were performed
121 following Agilent One-color Microarray-Based Gene Expression Analysis-Low Input Quick
122 Amp Labelling kit v6.6 protocol. Arrays were scanned with a G2565A Microarray Scanner
123 System with SureScan High-Resolution Technology, and spot intensities were quantified
124 using Feature Extraction 11.5.1.1 (Agilent Technologies, Inc. Santa Clara, CA). Background
125 correction and inter-array normalization were performed with GeneSpring software v12.6.1
126 (Agilent Technologies). Gene expression summaries were created for each gene by averaging
127 all probe sets for each gene. All data analysis was conducted on gene-summarized data.
128 Processed data were subsequently filtered for significant detection (P-value ≤ 0.01).

129

130 Quantitative analyses of selected mRNA in subcutaneous AT was performed as previously
131 described [7]. Briefly, RNA was prepared from tissue samples using an RNeasy Lipid Tissue
132 Mini Kit (Izasa). The integrity of each RNA sample was checked by an Agilent Bioanalyzer
133 (Agilent Technologies). Total RNA was quantified by the use of a spectrophotometer
134 (GeneQuant; GE Healthcare) and reverse transcribed to cDNA using a High Capacity cDNA
135 Archive Kit (Applied Biosystems Inc., Madrid, Spain) according to the manufacturer's protocol.
136 Gene expression was assessed by real-time PCR using a LightCycler 480 Real-Time PCR

137 System (Roche Diagnostics) using TaqMan® technology suitable for relative gene expression
138 quantification.
139

140 **REFERENCES**

- 141 [1] Carabús A, Gispert M, Brun A, Rodríguez P, Font-i-Furnols M. In vivo computed
142 tomography evaluation of the composition of the carcass and main cuts of growing pigs
143 of three commercial crossbreeds. *Livest Sci* 2014;170:181–192.
144 DOI:10.1016/j.livsci.2014.10.005.
- 145 [2] Boada I, Spinola J, Rodriguez J, Martínez R. VisualPork towards the simulation of a
146 virtual butcher. II Workshop on the Use Of ... 2009.
- 147 [3] Bardera A, Martínez R, Boada I, Font-i-Furnols M. VisualPork towards the simulation of
148 a virtual butcher. FAIM I Conference of COST ... 2012.
- 149 [4] Val-Laillet D, Blat S, Louveau I, Malbert CH. A computed tomography scan application
150 to evaluate adiposity in a minipig model of human obesity. *Br J Nutr* 2010;104:1719–
151 1728. DOI:10.1017/S0007114510002667.
- 152 [5] Furnols MF I, Teran MF, Gispert M. Estimation of lean meat content in pig carcasses
153 using X-ray computed tomography and PLS regression. ... and Intelligent Laboratory ...
154 2009.
- 155 [6] Want EJ, Masson P, Michopoulos F, Wilson ID, Theodoridis G, Plumb RS, et al. Global
156 metabolic profiling of animal and human tissues via UPLC-MS. *Nat Protoc* 2013;8:17–
157 32. DOI:10.1038/nprot.2012.135.
- 158 [7] Jové M, Moreno-Navarrete JM, Pamplona R, Ricart W, Portero-Otín M, Fernández-
159 Real JM. Human omental and subcutaneous adipose tissue exhibit specific lipidomic
160 signatures. *FASEB J* 2014;28:1071–1081. DOI:10.1096/fj.13-234419.

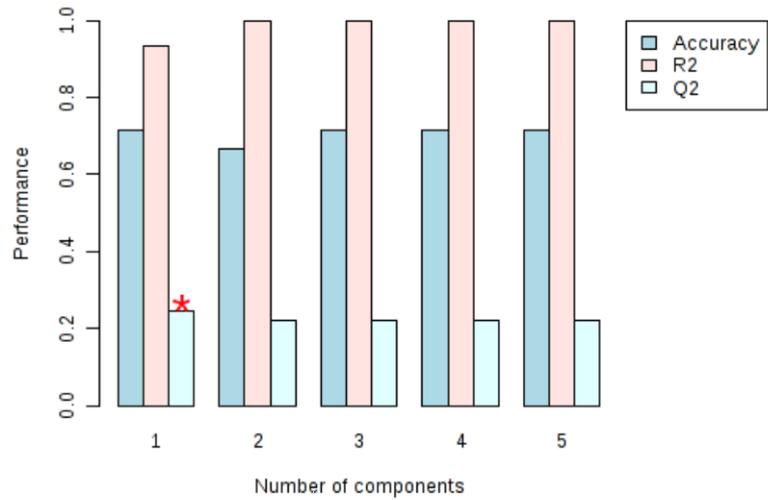
161

162

163

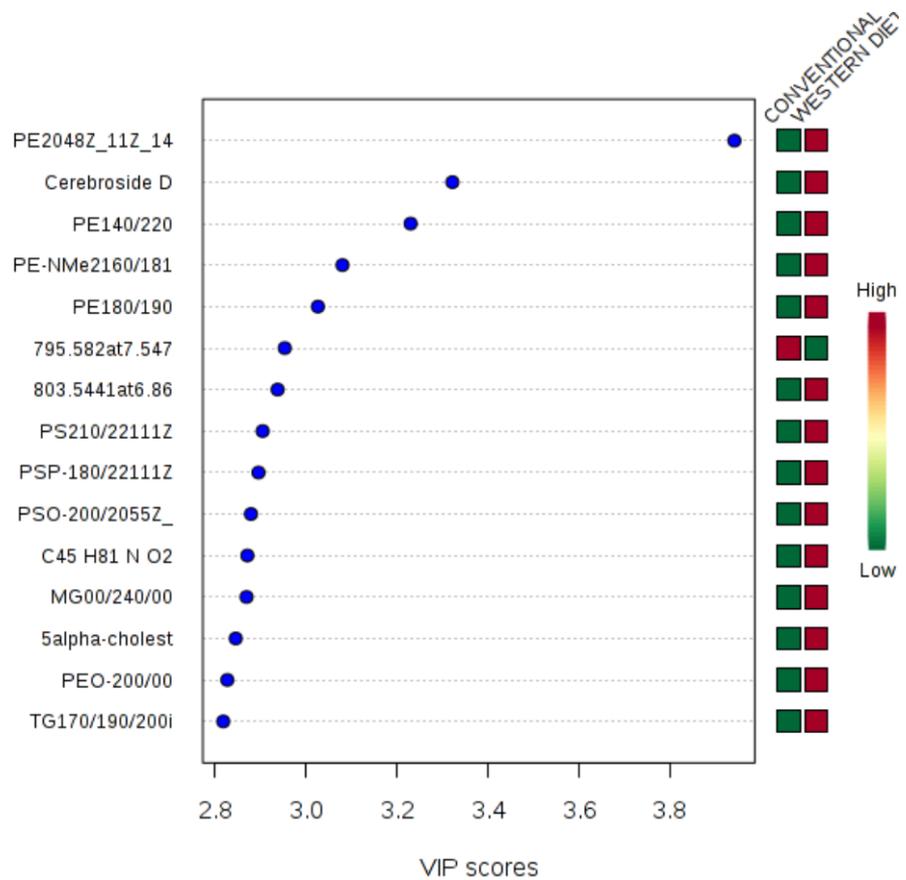
Supplemental Figure 1

A



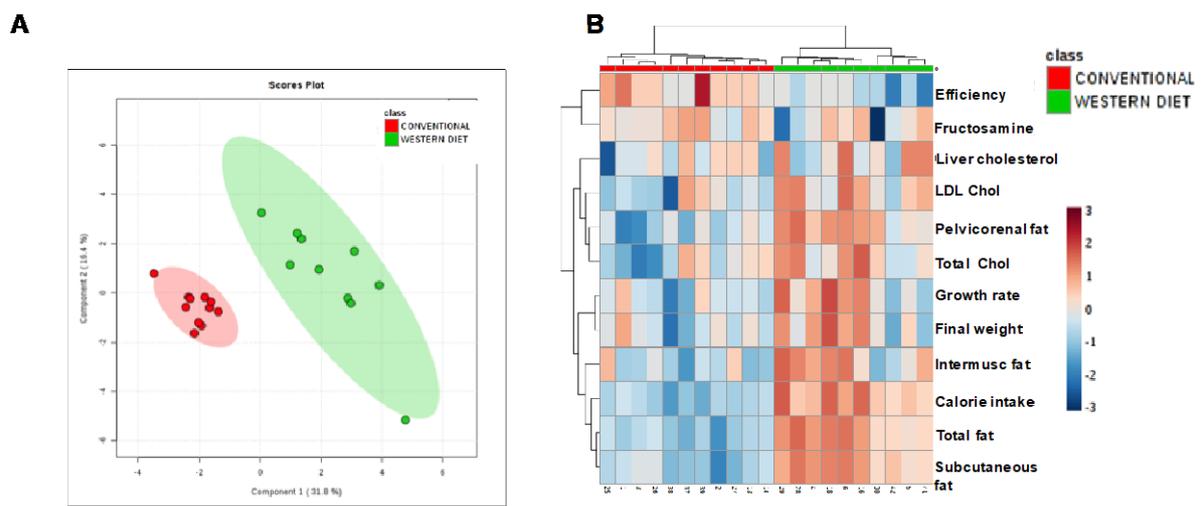
Measure	1 comps	2 comps	3 comps	4 comps	5 comps
Accuracy	0.71429	0.66667	0.71429	0.71429	0.71429
R2	0.93186	0.99808	0.99989	1.0	1.0
Q2	0.24573	0.22273	0.22017	0.2211	0.22109

B

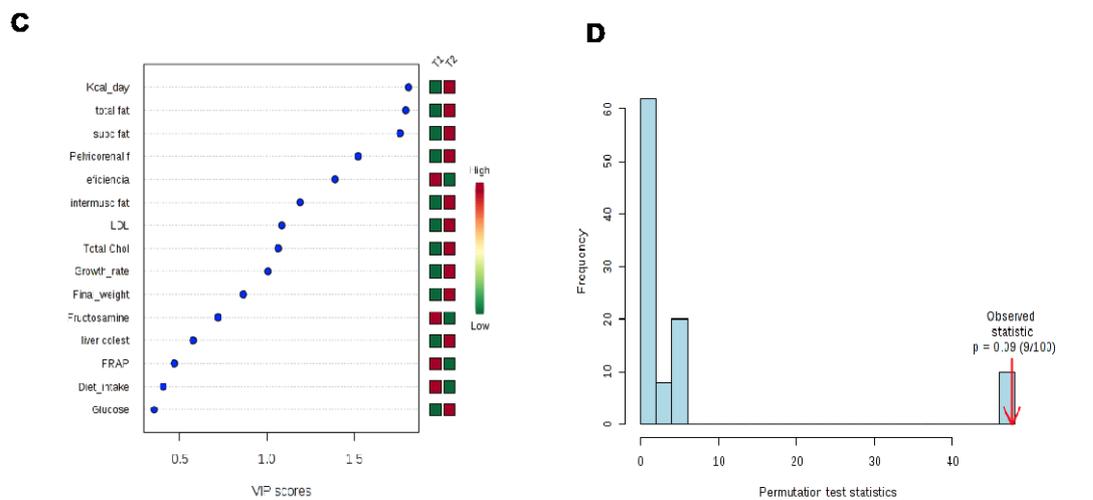


165 **Supplemental Figure 1.** Robustness of the PLS-DA model defining changes induced by a
 166 western-type diet (Figure 1 in the main text) is ensured by high accuracy, R2, and Q2 values.
 167 Variable importance in the projection of the first component demonstrates the importance of
 168 specific lipid molecules in plasma in helping to define a lipidomic signature associated with
 169 diet-induced obesity in prepubertal female pigs.

Supplemental Figure 2

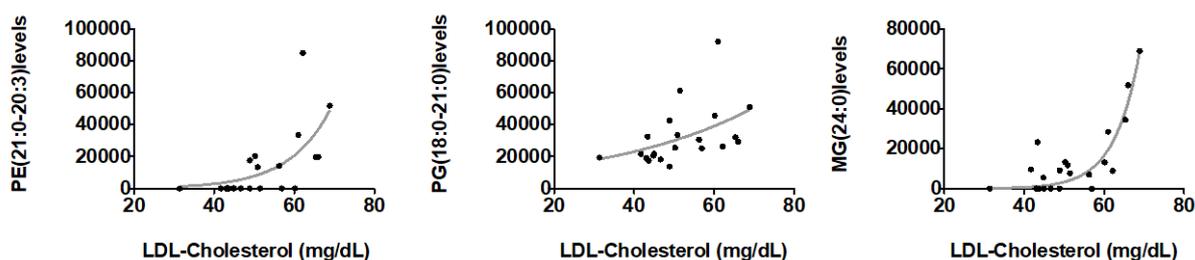


Measure	1 comps	2 comps	3 comps	4 comps	5 comps
Accuracy	0.95238	1.0	1.0	1.0	1.0
R2	0.82043	0.94066	0.96147	0.97133	0.98723
Q2	0.7679	0.87783	0.8926	0.89307	0.85764



171 **Supplemental Figure 2.** Biochemical and morphological traits define an obesity signature in
172 the proposed model of prepubertal obesity. A) PLS-DA model demonstrating a high accuracy
173 of the model, with more than 30% of variance being explained by the first component. B)
174 Hierarchical clustering and heatmap shows that conventional (clinical biochemistry) and CT
175 measures define a signature induced by western-type diet and demonstrate fat depot
176 segregation according to anatomical location and clusterization with biochemical traits. C)
177 Variable importance in projection (VIP) Scores of biochemical and morphological traits in the
178 first component of the PLS-DA model. D) Permutation test of the model, showing a global p-
179 value with a 0.09 value.

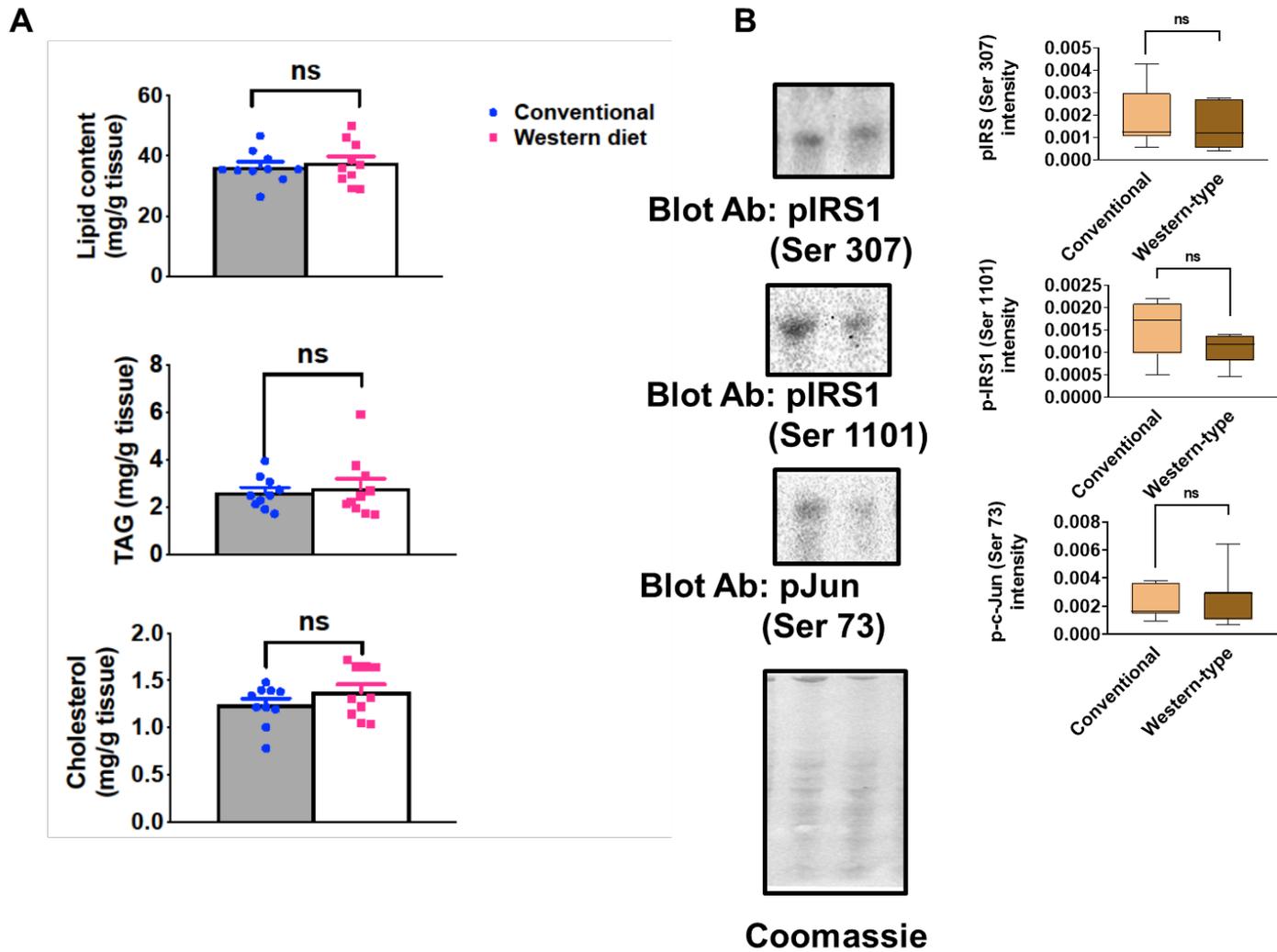
Supplemental Figure 3



180

181 **Supplemental Figure 3.** Plasma LDL cholesterol values are associated with specific plasma
182 lipids. Association of plasma concentration of selected lipids with LDL-cholesterol
183 concentration. Shown lipids are a selection from those showing a significant correlation with
184 specific traits (at least $p < 0.05$ by Spearman's rank correlation test, see Supplemental Data for
185 the whole list), while lines indicate non-linear fit (exponential growth equations;
186 $Y = Y_0 * \exp(k * X)$).

187



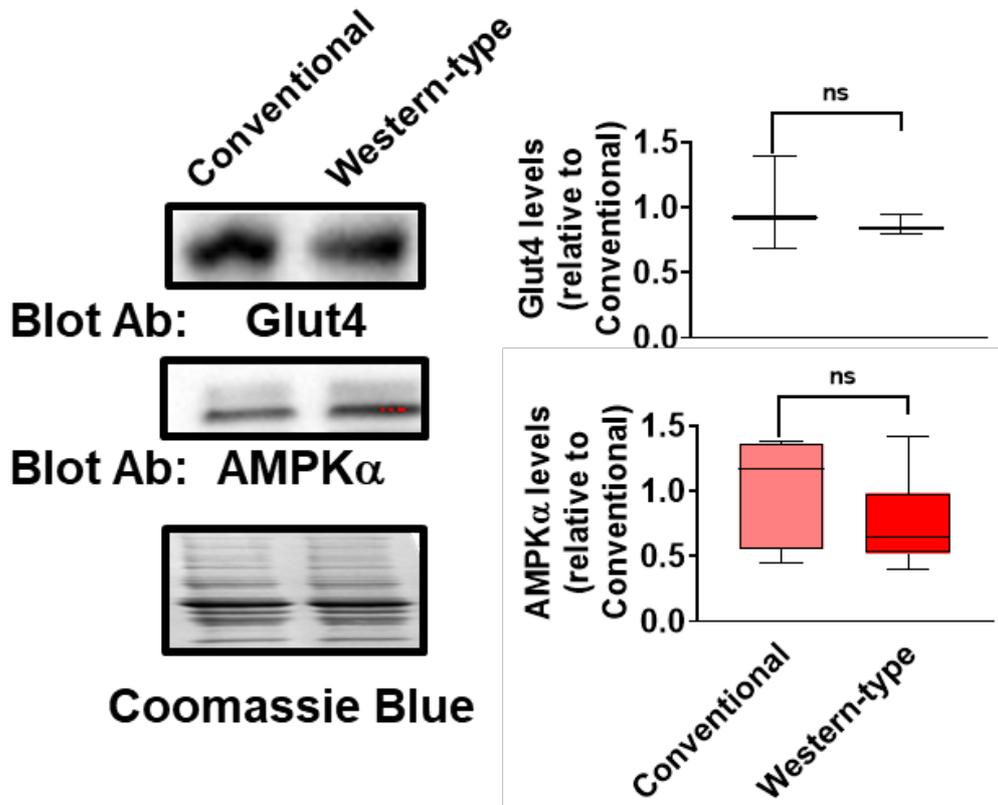
189

190 **Supplemental Figure 4.** A) Western-type diet does not increase lipid content in the liver,
191 nor triacylglyceride (TAG) concentrations or cholesterol levels B) shows a representative
192 western-blot of insulin-activity modulating signals in the liver and the influence of western-
193 type diet. Right graphs after each blot show densitometric integrated values normalized to
194 the total protein content, estimated by Coomassie blue staining, with p values after Students
195 t-test (n=6 for each group)

196

197

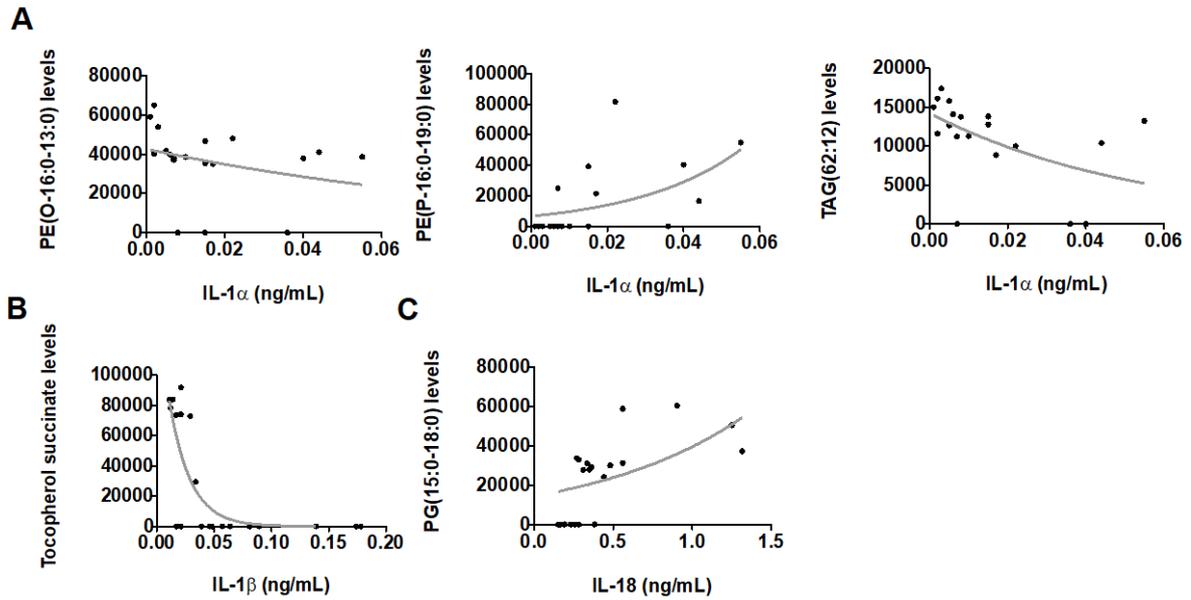
Skeletal muscle



198

199 **Supplemental Figure 5. Skeletal muscle insulin-responsive signals are not affected by**
200 **the western-type diet in the prepubertal model.** Representative western-blot of insulin-
201 responsive signals in skeletal muscle. Right graphs show densitometric integrated values,
202 normalized to the intensity of animals fed with conventional diets all adjusted to total protein
203 content, estimated by Coomassie blue staining, with p values after Students t-test

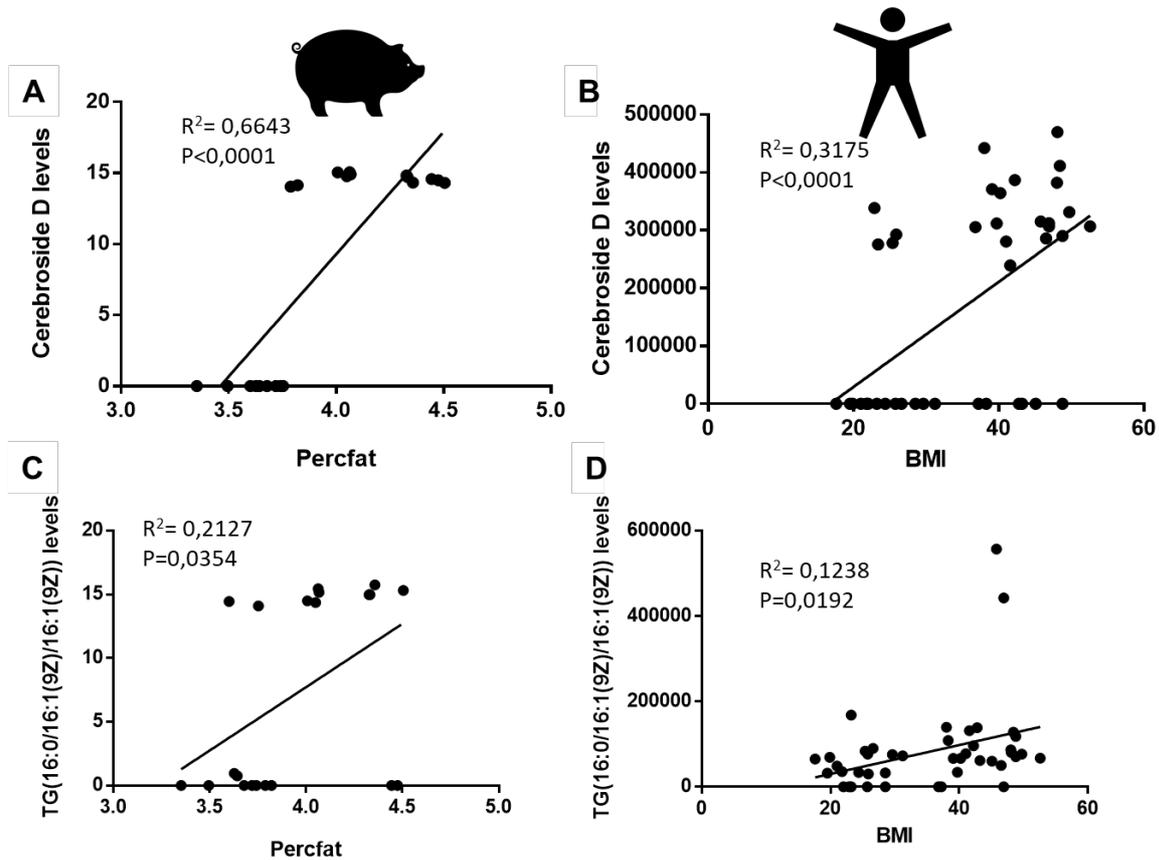
Supplemental Figure 6



204

205 **Supplemental Figure 6.** Peripheral markers of inflammation are associated with specific
206 plasma lipids. Association of plasma concentration of selected lipids with individual IL1a (A),
207 IL1b (B) and IL-18 (C) Shown lipids are a selection from those showing significant correlation
208 with specific traits (at least $p < 0.05$ by Spearman's rank correlation test, see Supplemental
209 Data for the whole list) while lines indicate non-linear fit (exponential growth equations;
210 $Y = Y_0 * \exp(k * X)$).

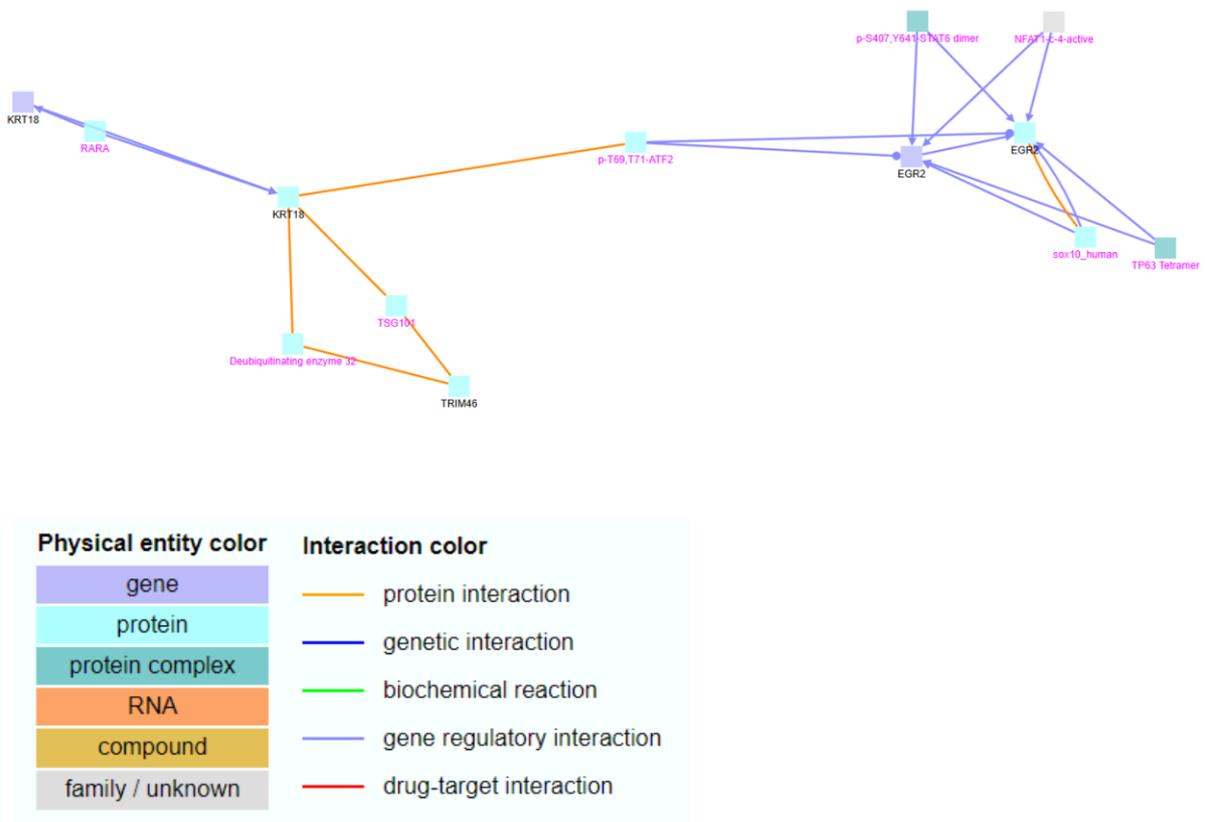
Supplemental Figure 7



212

213 **Supplemental Figure 7.** Validation in humans with obesity of proposed biomarkers. Specific
 214 lipids show a similar positive correlation with BMI (in humans, in B and D) and AT abundance
 215 (in the porcine model, in A and C).. All correlations are significant (at least $p < 0.05$) by
 216 Spearman's rank correlation test. Lines show the linear relationship, with R^2 and p values for
 217 linear adjustment shown in the inset. Pig icon comes from aLf; and Human one by Ma Qing
 218 both from the Noun Project (thenounproject.com)

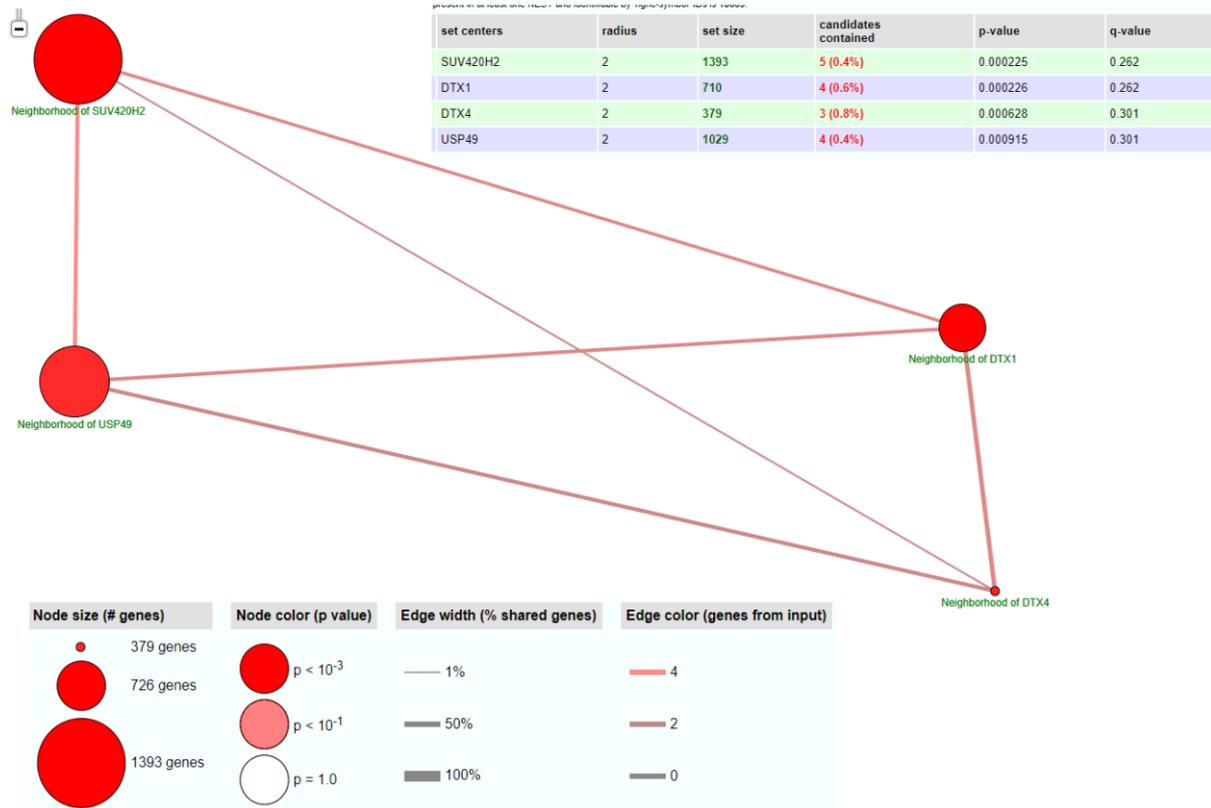
Supplemental Figure 8



219

220 **Supplemental Figure 8.** Induced network module analyses of PBMC transcriptomic changes
 221 associated with the western-type diet. Genes (see main text) were entered into the
 222 ConsensusPathDB platform, and interactions, coded by colors link nodes, representing
 223 entities (identified by colors). Black node labels denote genes significantly influenced by high-
 224 calorie diet, while magenta node labels denote intermediate nodes. All types of protein
 225 interactions (high to low confidence protein interactions) were considered, as well as genetic,
 226 biochemical, and gene regulatory interactions, with all available database sources in the
 227 platform being considered.

Supplemental Figure 9

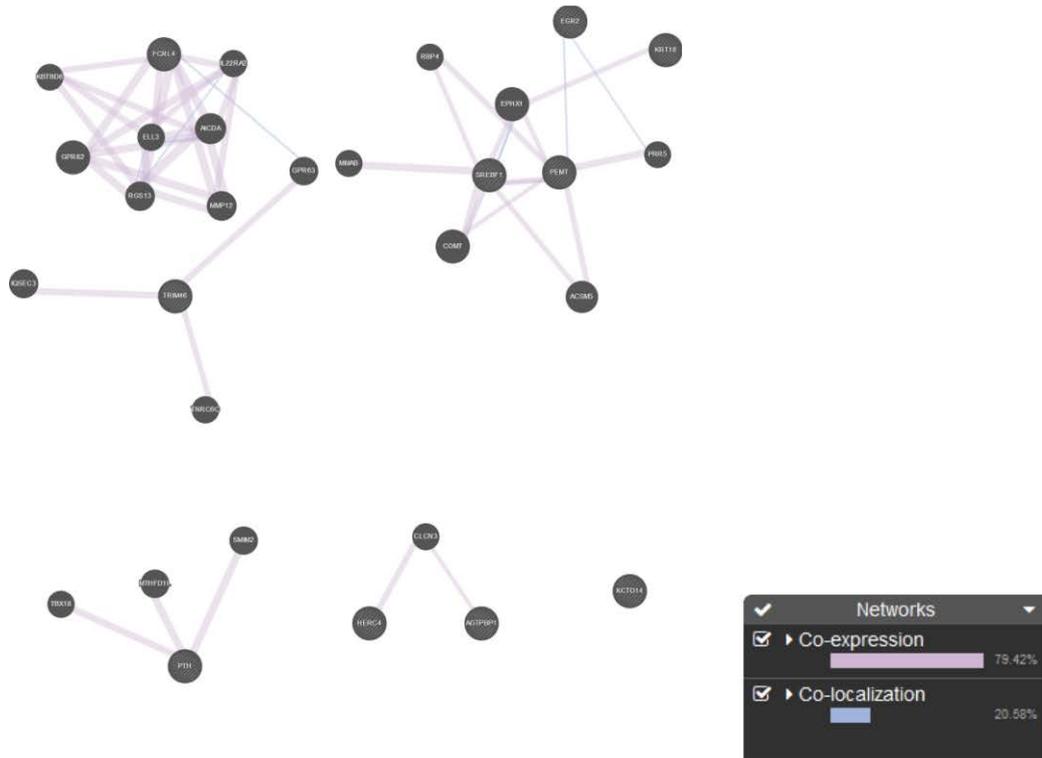


228

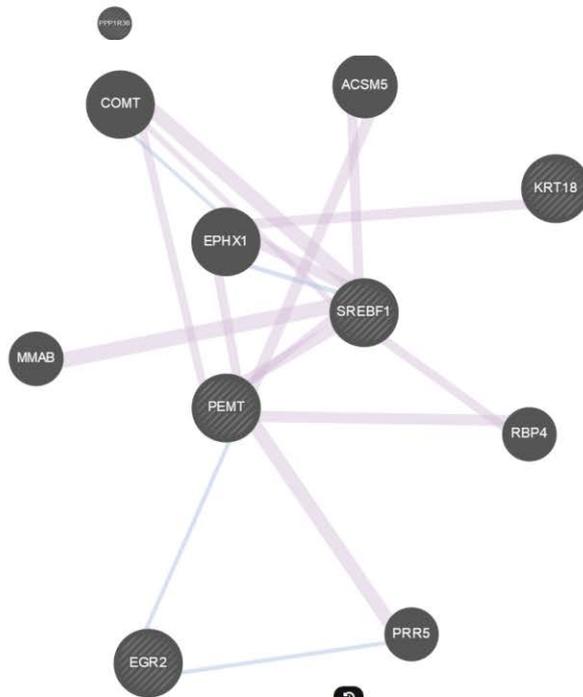
229 **Supplemental Figure 9.** Network neighborhood-based entity sets of PBMC transcriptomic
 230 changes associated with western-type diet. Genes (see main text) were entered into
 231 ConsensusPathDB platform, and nodes, representing neighborhood-based entity sets (whose
 232 size is proportional to the number of genes of the set, and color intensity denotes p-value for
 233 hypergeometric tests) are linked by interactions consisting of the number of genes shared by
 234 nodes. The type of network chosen was 2-next neighbors, with a minimum number of 2 genes
 235 from PBMC transcriptome overlap with members of the entity set (and a $p < 0.001$ as the cutoff).
 236 The sets were obtained considering only Reactome based ones, with gene ontology level 5
 237 categories and a p-value cutoff of 0.01 for ontology inclusion. The upper panel indicates the
 238 statistical values of each entity set.

Supplemental Figure 10

A



B



239

240

241 **Supplemental Figure 10.** Interatomic analyses of PBMC transcriptome changes.
242 Genes whose expression was changed by western-type diet in PBMC were introduced
243 into the Genemania platform, together with PEMT and SRBEP1, in order to evaluate
244 its potential clustering. The results (A) show five significant co-expression networks
245 and co-localization, with PEMT and SRBEP1 being localized into a network with EGR2
246 and KRT18.
247

248

249 **Supplemental Table 1.** Clinical characteristics of the cohort used for translational
250 applicability.

Parameter	Value ¹
N	44
Age	49.41±8.71
Gender	52% female
BMI (Kg/m ²)	35.04±10.7
Waist to hip ratio	0.90±0.11
HOMA-IR	3.08±3.07
Blood Cholesterol (mg/dL)	196.2±40.35
Blood LDL-Cholesterol (mg/dL)	122.9±34.6
Blood HDL-Cholesterol (mg/dL)	54.6±15.5
Glycemia (mg/dL)	94.2±12.5
Triacylglyceridemia (mg/dL)	95.5±49.49

251 ¹Values shown are mean±SD unless stated otherwise.

252

253 **Supplemental Table 2.** Composition of experimental diets applied from 9 to 11 weeks
254 of age

255

Component(%)	Conventional transition	Western-type transition
Oats	66.00	-
Wheat	-	42.00
Maize	-	16.00
Soy protein concentrate	-	-

Hydrolyzed rice protein	-	-
Caseinate	10.96	9.88
Starch	1.00	10.00
Saccharose	-	5.00
Wheat bran	15.00	4.00
Soybean hulls	4.10	-
Lard	-	10.00
Dicalcium phosphate	1.18	1.52
Calcium carbonate	0.98	0.51
Salt	0.35	0.37
L-Lysine-HCl	-	0.19
L-Threonine	-	0.03
DL-Methionine	-	0.10
L-Tryptophan	-	-
Ethoxiquin	0.02	0.02
Vit-Min complex (*)	0.40	0.40

256 (*) Provides per kg feed: vitamin A (E-672) 5500 UI; vitamin D3 (E-671) 1100 UI; vitamin E (alfa-tocopherol) 7 mg; vitamin B1 0.5
257 mg; vitamin B2 1.4 mg; vitamin B6 1 mg; vitamin B12 8 µg; vitamin K3 0.5 mg; calcium panthotenate 5.6 mg; nicotinic acid 8 mg;
258 choline 120 mg; Fe (E-1) (from FeSO4·7H2O) 80 mg; I (E-2) (from Ca(I2O3)2) 0.5 mg; Co (E-3) (from 2CoCO3·3Co(OH)2·H2O)
259 0.4 mg; Cu (E-4) (from CuSO4·5H2O) 5 mg; Cu (E-4) (from amino acids quelate) 5 mg; Mn (E-5) (from MnO) 40 mg; Zn (E-6)
260 (from ZnO) 100 mg; Se (E-8) (from Na2SeO3) 0.25 mg.

261 **Supplemental Table 3.** Nutritional composition of experimental diets applied from 9
262 to 11 weeks of age

Amount (%)	Conventional transition	Western-type transition
Crude Protein	17.98	15.55
Crude Fibre	12.20	1.68
Fat	4.98	11.80
Ash	5.96	4.15

Sodium	0.15	0.15
Chloride	0.29	0.31
Total calcium	0.86	0.70
Total phosphorous	0.58	0.49
Digestible phosphorous	0.27	0.27
Lysine	1.11	1.03
Threonine	0.75	0.65
Methionine	0.41	0.44
Met+Cys	0.69	0.64
Tryptophan	0.26	0.22
Energy (MJ ME/kg)	10.42	15.39

263

264 **Supplemental Table 4.** Composition of experimental diets applied from 12 to 19

265 weeks of age

Component(%)	Conventional	Western-type
Oats	55.28	-
Wheat	-	45.87
Maize	-	13.56
Caseinate	9.76	8.54
Starch	13.13	10.00
Saccharose	-	5.00
Wheat bran	15.00	4.00
Soybean hulls	4.00	-
Lard	-	10.00
Dicalcium phosphate	1.27	1.51

Calcium carbonate	0.78	0.51
Salt	0.36	0.37
Ethoxyquin	0.02	0.02
L-Lysine-HCL	-	0.15
L-Threonine	-	0.01
DL-Methionine	0.003	0.07
Vit-Min complex (*)	0.40	0.40

266 (*) Provides per kg feed: vitamin A (E-672) 5500 UI; vitamin D3 (E-671) 1100 UI; vitamin E (alfa-tocopherol) 7 mg; vitamin B1 0.5 mg;
267 vitamin B2 1.4 mg; vitamin B6 1 mg; vitamin B12 8 µg; vitamin K3 0.5 mg; calcium panthotenate 5.6 mg; nicotinic acid 8 mg; choline 120
268 mg; Fe (E-1) (from FeSO4·7H2O) 80 mg; I (E-2) (from Ca(I2O3)2) 0.5 mg; Co (E-3) (from 2CoCO3·3Co(OH)2·H2O) 0.4 mg; Cu (E-4)
269 (from CuSO4·5H2O) 5 mg; Cu (E-4) (from amino acids quelate) 5 mg; Mn (E-5) (from MnO) 40 mg; Zn (E-6) (from ZnO) 100 mg; Se (E-8)
270 (from Na2SeO3) 0.25 mg.

271

272

273 **Supplemental Table 5.** Nutritional composition of experimental diets applied from 12
274 to 19 weeks of age

Amount(%)	Conventional	Western-type
Protein	17.6	14.34
Fat	4.6	11.55
Fiber	11	1.72
Sodium	0.15	0.15
Chloride	0.29	0.31
Calcium	0.80	0.70
Total phosphorous	0.56	0.49
Digestible phosphorous	0.27	0.27
Lysine	0.99	0.90
Threonine	0.66	0.57
Methionine	0.36	0.37
Met+Cys	0.61	0.56
Tryptophan	0.23	0.20
Ash	5.55	4.13
Energy (MJ/ kg)	10.83	15.16

275

276

277

278

279 **Supplemental Table 6.** Antibodies and conditions.

280

Antigen	Supplier	Reference	Dilution
GLUT2	Abcam	ab104622	1:1000
SREBP1	Abcam	ab3259	1:1000
GLUT4	Invitrogen	MA1-83191	1:1000
AMPK α	Invitrogen	PA5-17398	1:1000
Phospho-IRS1 (Ser 307)	Upstate	07-247	1:1000
Phospho-IRS1 (Ser 1101)	Cell Signaling	2385	1:300
Phospho-c-JUN (Ser73)	Cell Signaling	3270	1:1000
anti-mouse IgG	Amersham	NA931V	1:30000
anti-rabbit IgG	Pierce	31460	1:100000

281

282

Compound	Reference		
1,3(<i>d5</i>)-dihexadecanoyl-glycerol	110537, Lipids	Avanti	Polar
1,3(<i>d5</i>)-dihexadecanoyl-2-octadecanoyl-glycerol	110543, Lipids	Avanti	Polar
1-hexadecanoyl(<i>d31</i>)-2-(9Z-octadecenoyl)-sn-glycero-3-phosphate	110920, Lipids	Avanti	Polar
1-hexadecanoyl(<i>d31</i>)-2-(9Z-octadecenoyl)-sn-glycero-3-phosphocholine	110918, Lipids	Avanti	Polar
1-hexadecanoyl(<i>d31</i>)-2-(9Z-octadecenoyl)-sn-glycero-3-phosphoethanolamine	110921, Lipids	Avanti	Polar
1-hexadecanoyl-2-(9Z-octadecenoyl)-sn-glycero-3-phospho-(1'-rac-glycerol-1',1',2',3',3'- <i>d5</i>)	110899, Lipids	Avanti	Polar
1-hexadecanoyl(<i>d31</i>)-2-(9Z-octadecenoyl)-sn-glycero-3-phospho-myo-inositol	110923, Lipids	Avanti	Polar
1-hexadecanoyl(<i>d31</i>)-2-(9Z-octadecenoyl)-sn-glycero-3-[phospho-L-serine]	110922, Lipids	Avanti	Polar
26:0- <i>d4</i> Lyso PC	860389, Lipids	Avanti	Polar
18:1 Cholesterol (<i>d7</i>) ester	111015, Lipids	Avanti	Polar
cholest-5-en-3 β -ol(<i>d7</i>)	LM-4100, Lipids	Avanti	Polar

D-erythro-sphingosine- <i>d7</i>	860657,	Avanti	Polar
	Lipids		
D-erythro-sphingosine- <i>d7</i> -1-phosphate	860659,	Avanti	Polar
	Lipids		
N-palmitoyl- <i>d31</i> -D-erythro-sphingosine	868516,	Avanti	Polar
	Lipids		
N-palmitoyl- <i>d31</i> -D-erythro-sphingosylphosphorylcholine	868584,	Avanti	Polar
	Lipids		
Octadecanoic acid-2,2- <i>d2</i>	19905-58-9,	Sigma Aldrich	

285

286

287

288 **Supplemental Table 8** . Changes in subcutaneous AT mRNA concentration induced
 289 by the western-type diet.

290

<i>Gene</i>	Conventional ¹	Western-type	Change (%)	p-value
<i>lep</i>	0.0225 ± 0.0152	0.064 ± 0.0215	184.8	<0.00001
<i>Il6</i>	0.0072 ± 0.0079	0.0032 ± 0.0015	-55.7	0.15
<i>Irs1</i>	0.0635 ± 0.0291	0.0464 ± 0.0199	-26.9	0.158
<i>fasn</i>	5.4763 ± 1.732	5.5608 ± 1.4093	1.5	0.908
<i>adipoq</i>	126.87 ± 71.05	94.71 ± 34.74	-25.3	0.211
<i>Insr1</i>	1.05 ± 0.22	1.13 ± 0.22	7.6	0.455
<i>gapdh</i>	17.77 ± 4.53	20.9 ± 7.29	17.6	0.247

291 ¹Values shown are mean±SD unless stated otherwise.

292

293

294 **Supplemental Table 9.** Changes in plasma interleukine concentration induced by the
295 western-type diet.

Parameter (pg/mL)	Conventional	Western-type	p ¹
IL-1a	0.016.9±0.014	0.014±0.019	0.9
IL-1b	0.054±0.047	0.056±0.061	0.9
IL-1ra	0.13±0.12	0.11±0.11	0.6
IL-10	0.08±0.12	0.09±0.16	0.9
IL-18	0.43±0.31	0.48±0.36	0.9

296

297 Values shown are mean±SD unless stated otherwise. ¹Student's t-test comparison
298 between values in conventional and western-type diets

299

300 **Supplemental Table 10.** Changes in plasma metabolome induced by western-type
 301 diet

Compound	Log FC	p	p (Corr)	Regulation (Conventional versus western-type)	FC (Control vs High Calorie)
Leucine	-0.44	8.22E-04	2.73E-02	Up	1.36
Pantheine	-1.35	1.51E-04	8.38E-03	Up	2.55
N-ethylarachidonoyl amine	-14.73	2.16E-04	1.09E-02	Up	27116.81
N-Lignoceroylsphingosine	-0.94	9.37E-04	3.01E-02	Up	1.92
3alpha,6alpha,7alpha,12alpha-Tetrahydroxy-5beta-cholest-24-en-26-oic acid	13.93	1.30E-05	9.63E-04	Down	-15602.22
GlnMetGln	14.47	4.82E-08	6.85E-06	Down	-22617.46

302
 303
 304

Figure 2 whole western blots

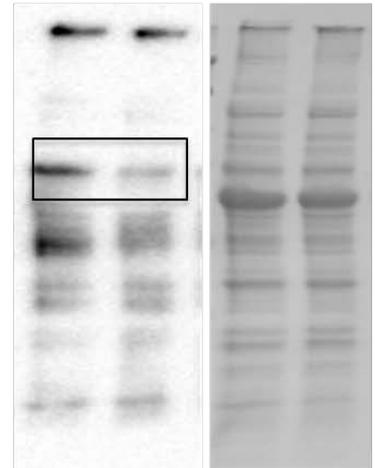
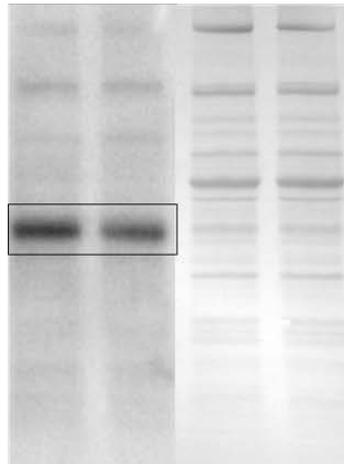
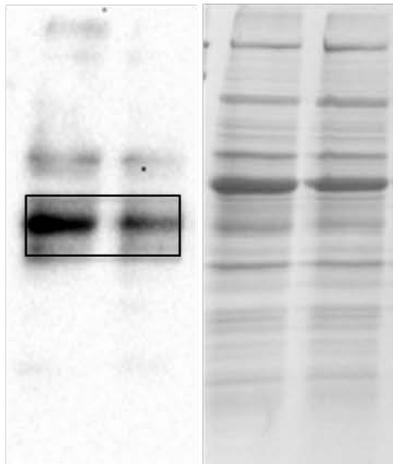
Glut4 Oment Glut4 Subcut

Glut2 PelvRen

Conventional
Western-type

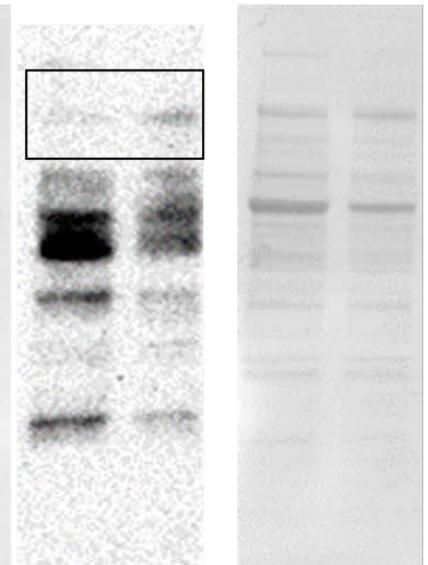
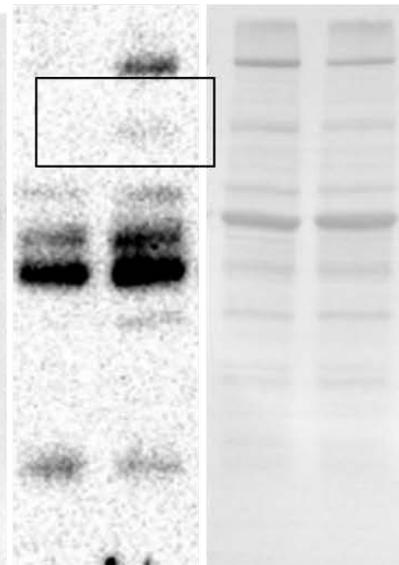
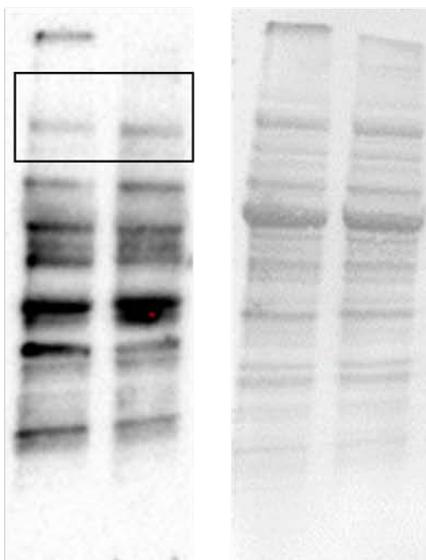
Conventional
Western-type

Conventional
Western-type



Srbep1 Subcut Srbep1 Oment

Srbep1 PelvRen



AMPK Subcut AMPK Oment

AMPK PelvRen

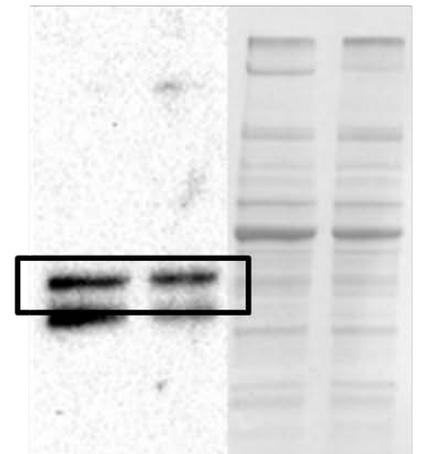
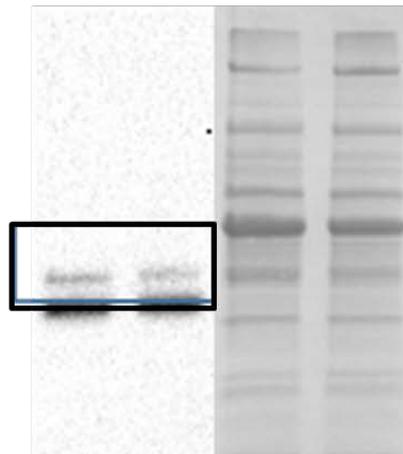
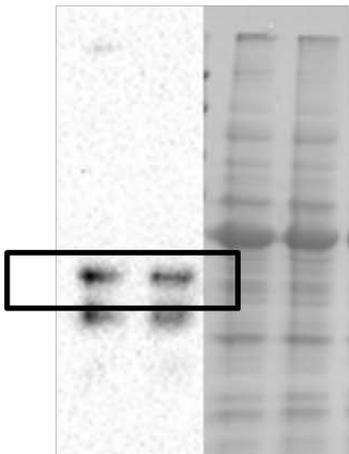
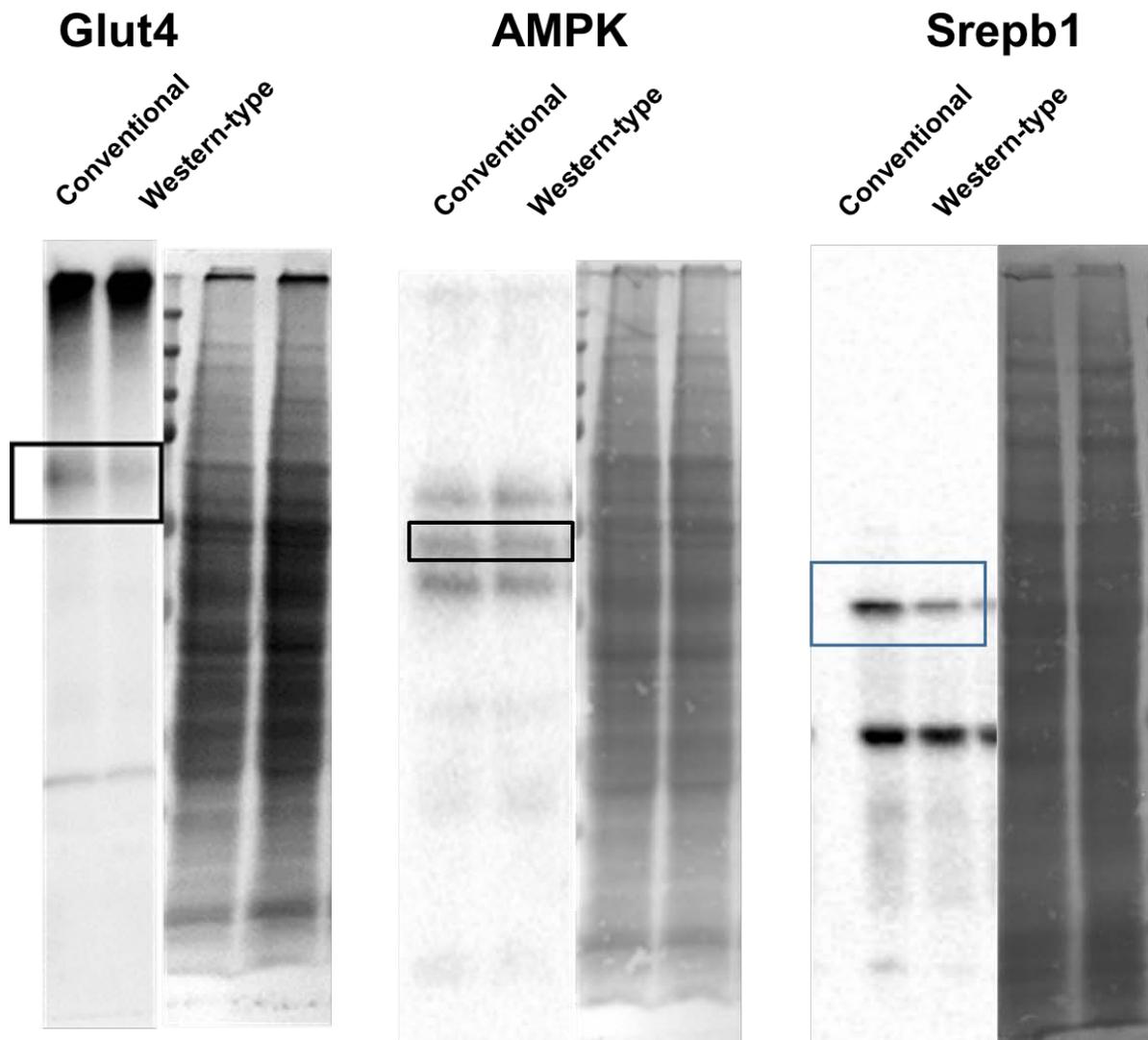
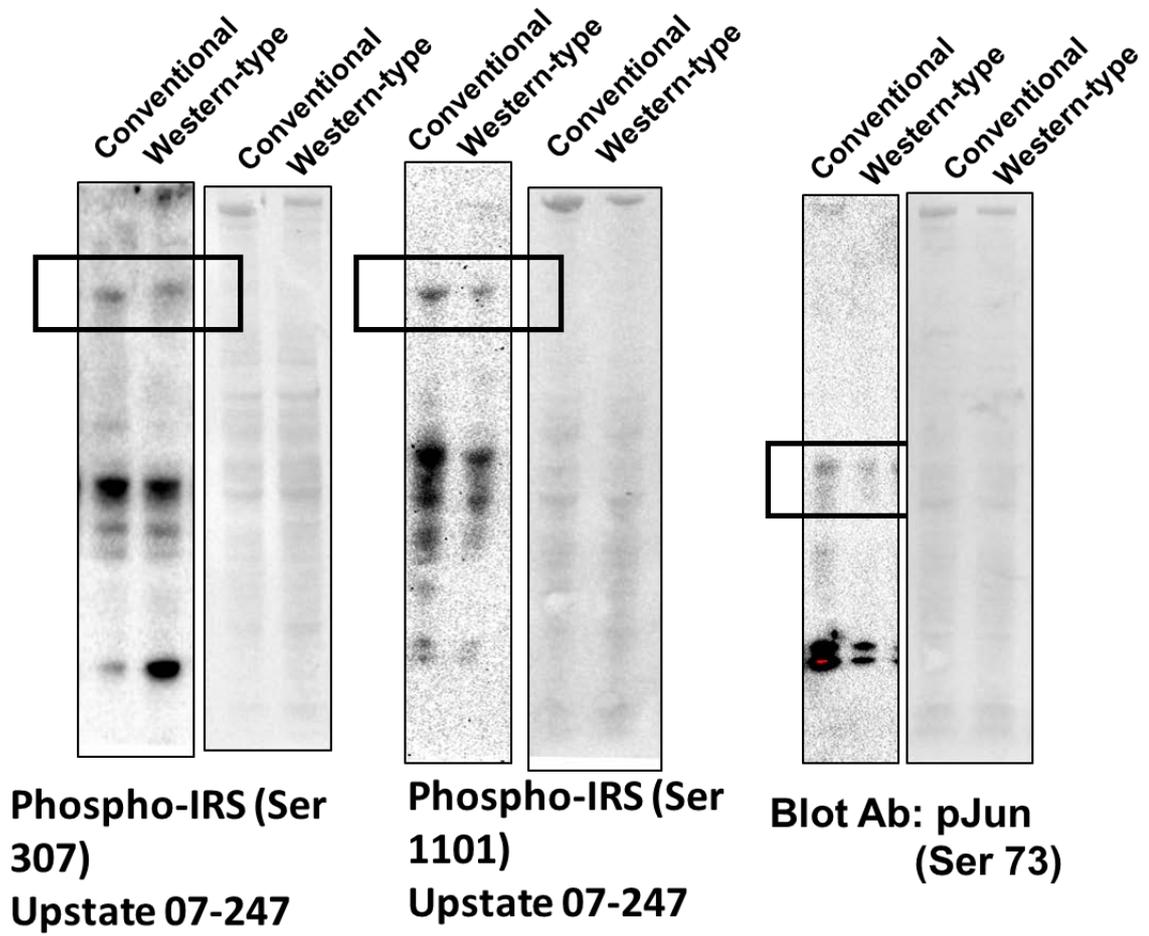


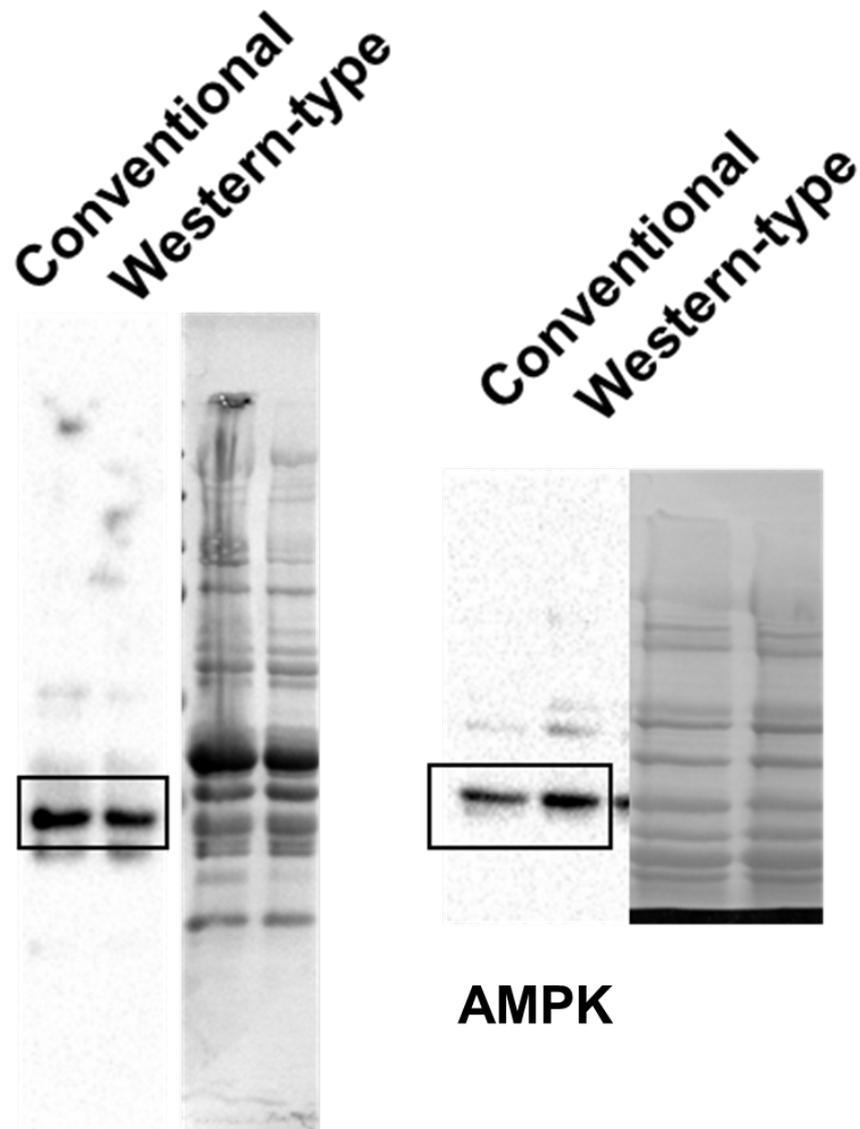
Figure 4 whole western blots



Supplemental Figure 4 whole western blots



Supplemental Figure 5 whole western blots



Glut4

AMPK